

UNCLASSIFIED

AD NUMBER

AD921719

LIMITATION CHANGES

TO:

Approved for public release; distribution is unlimited.

FROM:

Distribution authorized to U.S. Gov't. agencies only; Test and Evaluation; OCT 1973. Other requests shall be referred to Air Force Avionics Laboratory, Attn: TEO, Wright-Patterson AFB, OH 45433.

AUTHORITY

AFAL ltr, 20 Jan 1976

THIS PAGE IS UNCLASSIFIED

**Best Available
Copy
for all Pictures**

THIS REPORT HAS BEEN DELIMITED
AND CLEARED FOR PUBLIC RELEASE
UNDER DOD DIRECTIVE 5200.20 AND
NO RESTRICTIONS ARE IMPOSED UPON
ITS USE AND DISCLOSURE.

DISTRIBUTION STATEMENT A

APPROVED FOR PUBLIC RELEASE;
DISTRIBUTION UNLIMITED.

AFAL-TR-73-94
PART III



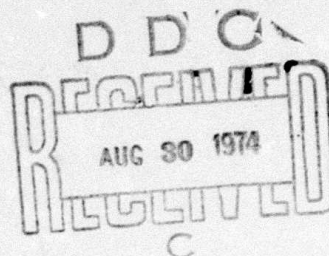
AD921719

0.85 MICRON SOLID STATE LASER MATERIAL EVALUATION

E.P. Chicklis, D.R. Gabbe, R.C. Folweiler, C.S. Naiman, et al
SANDERS ASSOCIATES, INC. — DEFENSIVE SYSTEMS DIVISION
(603) 885-3010

TECHNICAL REPORT AFAL-TR-73-94, PART III

JUNE 1974



DISTRIBUTION LIMITED TO UNITED STATES GOVERNMENT AGENCIES ONLY; BY REASON OF INCLUSION OF TEST AND EVALUATION DATA; APPLIED OCTOBER 1973. OTHER REQUESTS FOR THIS DOCUMENT MUST BE REFERRED TO AFAL/TEO, WRIGHT-PATTERSON AFB, OHIO 45433.

AIR FORCE AVIONICS LABORATORY — AIR FORCE SYSTEMS COMMAND
Wright-Patterson Air Force Base, Ohio 45433

NOTICE

When Government drawings, specifications, or other data are used for any purpose other than in connection with a definitely related Government procurement operation, the United States Government thereby incurs no responsibility nor any obligation whatsoever; and the fact that the government may have formulated, furnished, or in any way supplied the said drawings, specifications, or other data, is not to be regarded by implication or otherwise as in any manner licensing the holder or any other person or corporation, or conveying any rights or permission to manufacture, use, or sell any patented invention that may in any way be related thereto.

Copies of this report should not be returned unless return is required by security considerations, contractual obligations, or notice on a specific document.

AFAL-TR-73-94
PART III

0.85 MICRON SOLID STATE LASER MATERIAL EVALUATION

E.P. Chicklis, D.R. Gabbe, R.C. Folweiler, C.S. Naiman, et al

DISTRIBUTION LIMITED TO UNITED STATES GOVERNMENT AGENCIES ONLY; BY REASON OF
INCLUSION OF TEST AND EVALUATION DATA; APPLIED OCTOBER 1973. OTHER REQUESTS
FOR THIS DOCUMENT MUST BE REFERRED TO AFAL/TEO, WRIGHT-PATTERSON AFB, OHIO 45433.

FOREWORD

This is the third semi-annual report on Contract F33615-72-C-2065 and covering the work performed to evaluate the 0.85 micron solid state laser material Erbium:Yttrium Lithium Fluoride. This work is sponsored by Advanced Research Projects Agency under ARPA Order No. 2075, CLIN 0001. The amount of the contract is \$155,270. The inclusive dates of the research reported herein are 5 June 1973 to 5 January 1974.

This report was submitted on 29 April 1974. The work on the first two parts of the program is described in AFAL-TR-73-94 (Parts I and II). The first part does not have a part designation.

Mr. Richard L. Remski (TEO), Air Force Avionics Lab, Air Force Systems Command, Wright-Patterson Air Force Base, Ohio is the Project Monitor of this program.

These studies were carried out at Sanders Associates, Electro-Optics Division, Merrimack Facility. Subcontracting services were provided by the Center of Material Sciences and Engineering, Crystal Physics Laboratory, Department of Electrical Engineering, Massachusetts Institute of Technology.

Dr. C.S. Naiman, Manager - Laser Systems Department is the Project Supervisor and E.P. Chicklis and R.C. Folweiler are the principal investigators. Mr. J.C. Doherty assisted with the laser measurements and Mrs. S. Lichtensteiger the spectroscopic measurements. The subcontracting efforts were directed by Dr. A. Linz. Investigation of crystal growth phenomena and analysis was conducted by Dr. D.R. Gabbe. Crystals were grown by D.R. Gabbe and R. Mills. Dr. H.P. Jensen assisted with some of the spectroscopic measurements and analyses.

The views and conclusions contained in this document are those of the authors and should not be interpreted as necessarily representing the official policies, either expressed or implied, of the Advanced Research Projects Agency of the U.S. Government.

This technical report has been reviewed and approved for publication.


AMOS H. DICKE, Chief
Electro-Optics Device Branch
Electronic Technology Division

ABSTRACT

This third semi-annual report describes the final phase of the program for the development of a 0.85 micron optically pumped laser material: $\text{Er}^{3+}:\text{YLF}$. Laser operation is obtained at room temperature in this material via stimulated $^4\text{S}_{3/2} \rightarrow ^4\text{I}_{13/2}$ transitions. $\text{Er}:\text{YLF}$ is a true four-level laser.

The relationship between growth parameters and feed purity and their effects on crystalline quality were investigated. Dramatic improvement in optical quality was obtained in growth runs using argon as the furnace cover gas. Preliminary evidence of further improvements in crystalline quality (comparable to $\text{Nd}:\text{YAG}$) resulted from the use of recrystallized feed.

The physical properties of YLF are reviewed and the results applied to a calculation of the thermal loading at fracture of a YLF rod uniformly heated and cooled at the surface. The calculated value is 11 watts/cm at thermal fracture corresponding to predicted output power of 7.6 watts/cm.

Spectroscopic studies focused on the effects of increased Er^{3+} concentration on laser efficiency. The temperature and concentration dependence of the lifetime of the upper laser level were measured. In flashpumped operation at room temperature an optimum concentration of approximately 5% is predicted.

Comparative measurements show significantly improved laser efficiency with Er^{3+} concentration over the range 2-3.5%. Improved laser performance was observed using rods grown in argon. A maximum output power of 0.8 watts at 25 Hz and a maximum repetition rate of 50 Hz was observed. For a 0.25 x 3 inch rod in excess of 2 watts are obtained by scaling the output with active volume. Overall efficiencies greater than 0.5% at 10 Hz are extrapolated from laboratory data.

(THIS PAGE INTENTIONALLY LEFT BLANK)

TABLE OF CONTENTS

<u>Section</u>	<u>Page</u>
1 INTRODUCTION AND SUMMARY	1
1.1 Accomplishments	1
2 CRYSTAL GROWTH	3
2.1 Crystals Grown	3
2.2 Crystalline Quality	4
2.2.1 Bubbles	10
2.2.2 Microscopic Scattering Inclusions	10
2.2.3 Refractive Index Defects	11
2.3 Crystalline Purity	11
2.3.1 Absorption Spectra	11
2.4 Discussion	15
2.4.1 Effects of Growth Parameters	15
2.4.1.1 Furnace Gas	15
2.4.1.2 Pulling and Rotation Rates	16
2.4.1.3 Thermal Effects	16
2.4.2 Feed Purity	17
3 PHYSICAL PROPERTIES	23
3.1 Thermal Conductivity	23
3.2 Modulus of Elasticity, Rupture and Poisson's Ratio	23
3.3 Thermal Expansion	23

TABLE OF CONTENTS (Cont)

<u>Section</u>	<u>Page</u>
3.4	Hardness 25
3.5	Density and Lattice Size 25
3.6	Optical Properties 25
3.7	Estimated Power Loading at Fracture 26
4	SPECTROSCOPY 31
4.1	Concentration Quenching 33
4.2	Temperature Dependence 34
5	LASER MEASUREMENTS 39
5.1	Effects of Er ³⁺ Concentration 40
5.1.1	Remarks 42
5.2	Repetitively Pulsed Operation 44
5.2.1	Rod 463.4:2.5% Er:YLF 44
5.2.2	Rod 446.1a:2% Er:YLF 48
5.2.3	Remarks 52
5.3	Q-Switching Experiments 52
5.4	Terminal Level Lifetime 53
6	PERFORMANCE POTENTIAL OF Er:YLF 55
6.1	Pumping Efficiency 55
6.2	Flourescence Lifetimes and Emission Cross Section 58
6.3	Threshold Parameters 58

TABLE OF CONTENTS (Cont)

<u>Section</u>		<u>Page</u>
6.4	Effects of Scattering on Laser Output	60
6.5	An Extrapolation	61
7.0	CONCLUSIONS AND RECOMMENDATIONS	65
	APPENDIX	67
	REFERENCES	71

LIST OF ILLUSTRATIONS

<u>Figure</u>		<u>Page</u>
1	YLF Boule 203f	5
2	He-Ne Scattering from Rod 458.1	6
3	YLF Boule 214f	7
4	YLF Boule 215f	8
5	YLF Boule 220f	9
6	View Through 7.5 cm of YLF	12
7	IR Transmission of Boule 214f	13
8	IR Transmission of Boule 215f	14
9	YLF Boule 199f	19
10	SEM Photo of 180f M = 420X, 2200X	21
11	SEM Photo of 180f	22
12	Energy Level Diagrams of Er:YLF and Nd:YAG	32
13	Time Dependence of $^4S_{3/2}$ Decay in Er:YLF	34
14	$^4S_{3/2}$ Decay Rate vs Concentration	36
15	$^4S_{3/2}$ Decay Rate and Lifetime vs Temperature	37
16	Laser Efficiency vs Er Concentration	41
17	Single Shot Output vs Input, Rod 463.4	46
18	Long Pulse Output Power vs Repetition Rate, Rod 463.4	47
19	Single Shot Output vs Input, Rod 446.1a	49
20	Long Pulse Output Power vs Input Energy, Rod 446.1a	50

LIST OF ILLUSTRATIONS (Cont)

<u>Figure</u>		<u>Page</u>
21	Long Pulse Output Power vs Repetition Rate, Rod 446.1a	51
22	Energy Level Diagrams of Er:YLF and Nd:YAG (Repeat of figure 12)	56
23	Absorption Spectra of Er:YLF and Nd:YAG	57
24	Effects of Scattering on Laser Output	62
25	Phase Diagram of the LiF-YF ₃ System	72
26	Phase Diagram of Congruently Melting LiReF ₄	75

LIST OF TABLES

<u>Table</u>		<u>Page</u>
I	Material and Optical Properties of YLF and YAG	24
II	Ultraviolet Absorption Edge of YLF.....	25
III	Physical Properties of YLF and YAG	29
IV	Thermal Loading at Fracture	29

1.0 INTRODUCTION AND SUMMARY

The results of the final six months of an eighteen month program to investigate the physical, spectroscopic, and laser properties of $\text{Er}^{3+}:\text{LiYF}_4$ (YLF) are presented. Laser oscillations at $0.85 \mu\text{m}$ are obtained in this optically pumped solid state material as the result of stimulated $^4\text{S}_{3/2} - ^4\text{I}_{13/2}$ transitions in the Er^{3+} ions. (1, 2) The objectives of this part of the program are:

- Improvement in the material optical quality.
- Growth of sufficient boules of repeatable optical quality for providing baseline data and determining the effects of composition in laser performance.
- Determination of fundamental performance limitations of the material.
- Measurement of laser performance in repetitively pulsed operation in the long pulse and Q-switched mode.

1.1 ACCOMPLISHMENTS

The major accomplishments during this phase of the program are summarized below.

- A dramatic improvement in the optical quality and yield of YLF rods has been obtained as the result of the use of argon (instead of helium) as the furnace gas. Four boules of approximate dimensions 1.5×7 cm were grown of uniform optical quality.
- The use of recrystallized LiYF_4 for feed material has resulted in the growth of a YLF boule which exhibited a complete absence of scattering centers when the scattered radiation of a He-Ne probe beam was viewed.

- Studies of the relationship between growth parameters and crystalline quality indicate an optimum pulling rate of 1.5 mm/hr.
- The effects of oxide in the melt have been investigated. Strong evidence that oxide is rejected from LiYF_4 as it crystallizes was obtained.
- Positive identification of bubble inclusions in a YLF crystal grown in He was obtained with scanning electron microscope. X-ray emission spectra did not reveal the presence of local impurity concentrations associated with inclusions.
- The lifetime of the upper laser level versus Er^{3+} concentration and temperature was measured. In flashpumped operation at room temperature an optimum concentration of $\sim 5\%$ is predicted based on the tradeoff between improved pumping efficiency and decreased storage time as the Er^{3+} concentration is increased. Very significant improvements in pumping efficiency and storage time can be obtained with higher Er^{3+} concentrations at lower temperatures.
- Based on measured thermal and mechanical properties of YLF the thermal load at fracture of a uniformly heated rod cooled only at the surface was determined to be 11 watts/cm at room temperature. The predicted laser power in flash pumped operation corresponding to this thermal loading is 7.6 watts/cm.
- Comparative laser measurements show significantly improved efficiency with increasing Er^{3+} concentration over the range 2 - 3.5%. The slope efficiency of a 3.5% Er:YLF rod was nearly twice that of a 2.5% rod of comparable optical quality.
- The improved quality of rods grown in an Argon atmosphere was substantiated by laser measurements. The highest output power observed previously with rods grown in an He atmosphere, was 0.25 watts. With the improved material up to 0.8 watts output was obtained. Scaling the output power proportional to active volume, we obtain 2.3 watts for a 0.25×3 inch rod (25 Hz).
- With only modest water flow rates (0.5 gal. min.) the output power was observed to equal the output observed in single shot operation at the same input energy times the pulse repetition rate at least up to 750 watts input (15 Hz).
- Reasonable extrapolations from observed data indicate overall operating efficiencies greater than 0.5% are obtainable.

2.0 CRYSTAL GROWTH

Crystals of Er:YLF ($\text{LiY}_{1-x}\text{Er}_x\text{F}_4$) were grown by the Top-Seeded Solution technique⁽³⁾, a modification of the Czochralski technique, in a highly purified inert atmosphere. A complete description of the growth technique is provided in references 4 and 5. The major focus of the work for this program was growth of Er:YLF boules of uniform optical quality for laser testing. In previous work (4), (6) definition of Er^{3+} :YLF laser performance and interpretation of laser performance of various Er^{3+} :YLF compositions was rendered somewhat ambiguous by a wide variation in material optical quality. Furthermore, the rod yield from previous boules was frequently severely limited due to local concentrations of large bubbles and bands of bubbles across the whole growth plane.

A major advance in the optical quality and yield of YLF boules has resulted from the use of argon as the furnace cover gas (instead of He). Five boules have been grown for this and other programs using Ar with complete absence of bubble type inclusions observed using a He atmosphere. Furthermore, the uniform quality of boules has eliminated the low rod yield/boule. Recent experiments using recrystallized feed have resulted in crystals with optical quality comparable to Nd:YAG, viz, complete absence of observable scattering under He-Ne illumination.

2.1 CRYSTALS GROWN

A summary of the boules grown during this phase of the program is described below. Boule 203f was grown in purified helium; the rest of the boules were grown in high purity commercial Ar.

203f LiYF_4 :2% Er, 0.5% Pr

This crystal was grown from zone refined Research Chemicals YF_3 and ErF_3 and zone refined Lindsay PrF_3 in an atmosphere of purified He. During the early stages of this run automatic diameter control was tested. It did not operate successfully and the boule had to be reseeded. The growth rate was maintained at 1 mm/hr requiring a temperature lowering rate of 0.7°C/hr on the average.

A uniform rotation rate of 40 RPM was used. A photograph of the boule is shown in figure 1. Four laser rods were obtained, two at 5×65 mm and two at 5×40 mm. Rod length was limited by the presence of bubble type inclusions and by the boule geometry. A photograph of the scattering from a He-Ne laser beam is shown in figure 2.

209f LiYF_4

A pure LiYF_4 boule was grown to replenish the stock of seed material.

214f LiYF_4 2.5% Er

This boule was grown from zone refined Lindsay YF_3 and ErF_3 . Two changes in growth conditions were introduced. Ar was used as the furnace atmosphere and the growth was at 1.5 mm/hr. The rotation rate was 40 RPM. The boule, figure 3, was bubble free. Four 6×60 mm rods were obtained after cutting top, bottom and sides to allow optical inspection. This represents virtually full utilization of the crystal. The optical quality was very good, and light scattering was visible only under He-Ne laser illumination.

215f LiYF_4 3.5% Er

This crystal was grown in Ar at a rate of 1.5 mm/hr. The boule is shown in figure 4. It was bubble free and exhibited scattering only under He-Ne laser illumination. Four rods, 48×5.5 mm each were obtained. Their length was limited by the constriction near the lower end of the boule.

218f LiYF_4 2% Er

This run was started with non-zone refined feed and was terminated after a brief time when the desired feed became available.

220f LiYF_4 2.5% Er 0.05% Pr

This boule, figure 5, was grown in Ar at 1.5 mm/hr from zone-refined Lindsey YF_3 and ErF_3 . The boule was characterized by a lack of bubbles and some scattering observable in He-Ne illumination. Four rods were obtained, three at 6×78 mm a fourth measuring 4×78 mm.

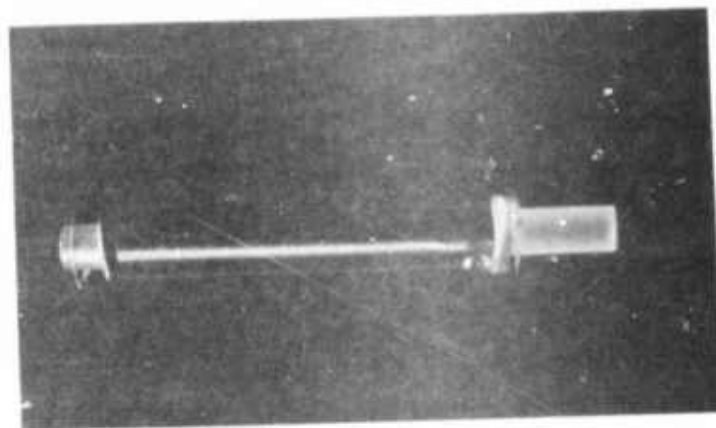
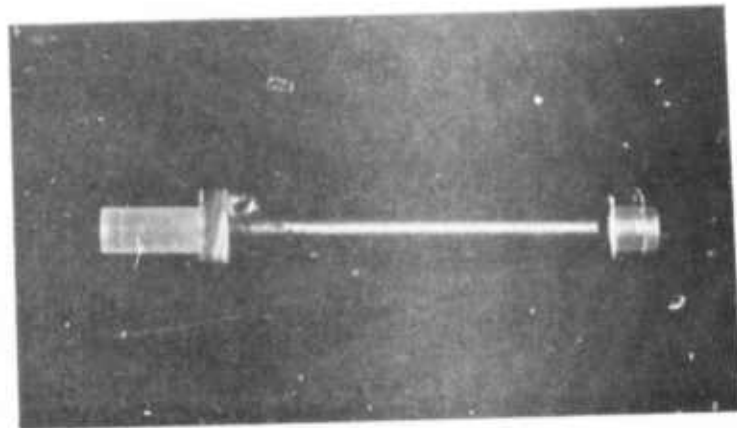
2.2 CRYSTALLINE QUALITY

The types of inclusions which have been observed in YLF crystals grown over the past five years have been categorized and are discussed below. Since in the past much of the growth was directed at spectroscopic investigation, the relationship between growth conditions and optical quality had not been systematically investigated. Spectroscopic studies have led to the development of various YLF room



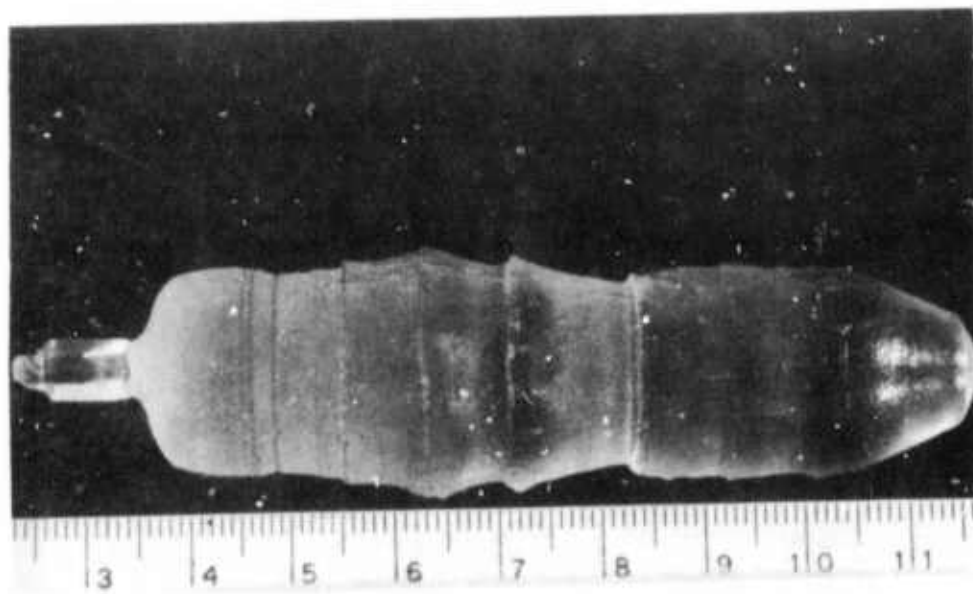
Figure 1 YLF Boule 203f.

2%Er - 0.5%Pr



D-144

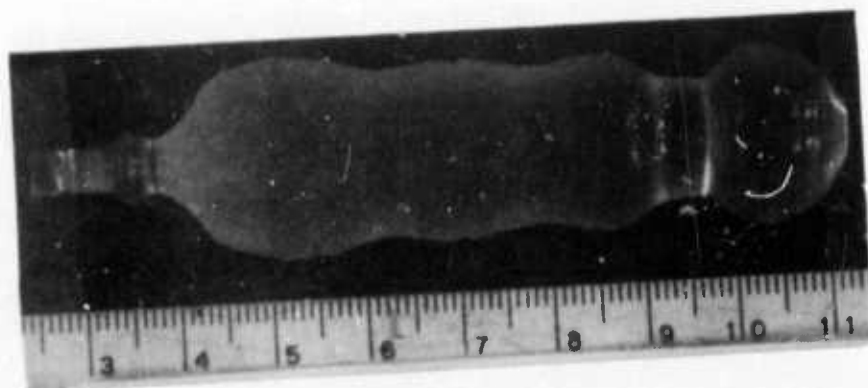
Figure 2 He-Ne Scattering for Rod 458.1 (Boule 203f).



214f $\text{LiYF}_4:2.5\% \text{Er}$

D-211

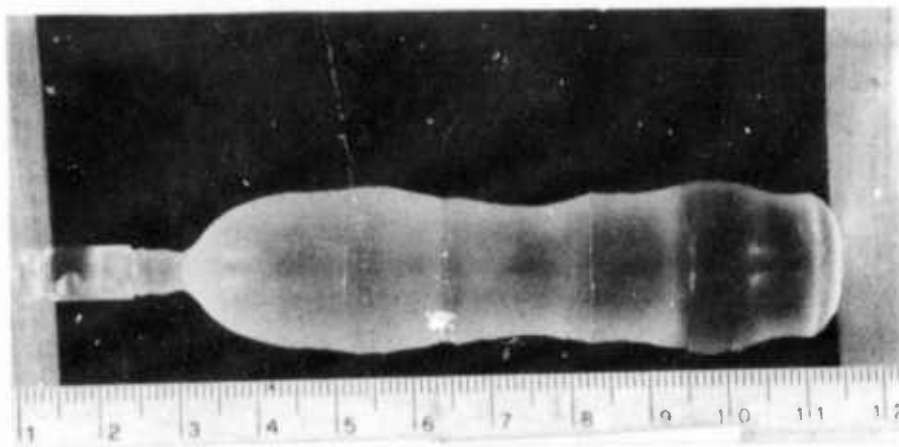
Figure 3 YLF Boule #214f.



215f LiYF_4 :3.5% Er

D-212

Figure 4 YLF Boule #215f.



220f LiYF_4 :2.5% Er - 0.05% Pr

D-213

Figure 5 YLF Boule #220f.

temperature lasers at wavelengths of 0.55⁽⁷⁾ 0.85,⁽¹⁾ 1.06,⁽⁸⁾⁽⁹⁾ 1.73,⁽²⁾ 2.06,⁽¹⁰⁾ and 2.8 μm ⁽¹¹⁾ which in turn has resulted in a demand for high optical quality boules.

2.2.1 BUBBLES

In prior growth runs using helium as the furnace gas isolated bubbles and bands of localized bubbles have been observed. The former type are generally isolated and frequently of elongated shape (order of tenths of millimeters in diameter) oriented parallel to the c-axis. The latter type are much smaller and frequently have formed in sufficiently high density to limit the useable length of the boule. Optical and scanning electron microscopy, SEM, (see Appendix II) analysis have confirmed that these types of inclusions are bubbles.

Until recently the major problem in YLF growth runs for laser rods has been the variable rod yield per boule due to local concentrations of large bubbles and bands of bubbles across the whole growth plane. These problems have apparently been eliminated with the use of argon as the furnace cover gas (instead of helium). Boules grown with an argon cover gas have exhibited excellent uniformity with nearly complete elimination of large bubbles and complete elimination of the bands of bubbles. This has been consistently observed in all the growth runs using Ar; a total of five large boules (each greater than 5 cm in length) has been grown on this and other programs.

2.2.2 MICROSCOPIC SCATTERING INCLUSIONS

What appears to be a fine precipitate has also been observed in some crystals. Sometimes this type of inclusion displays optical anisotropy, in other instances the precipitate appears as a light haze. The distribution of these types of defects is not uniform; their formation may be associated with a combination of impurities and thermal instabilities in the melt. The characterization of this type of defect as a "precipitate" may be misleading as this type of scattering center may consist partly of very fine bubbles.

It is emphasized that this type of inclusion is not visible to the unaided eye, requiring either He-Ne illumination with appropriate index matching or magnification.

Recently use of recrystallized feed material in a growth run in an argon atmosphere has resulted in a YLF boule with virtually none of the scattering inclusions discussed below. The optical quality of the boule was comparable to that of Nd:YAG when the scattered radiation of a He-Ne probe beam was viewed. This very exciting result does point to a relationship between inclusion formation and feed purity but additional studies are required.

2.2.3 REFRACTIVE INDEX DEFECTS

YLF crystals grown by this technique are characterized by very low strain. Some poor quality material has exhibited apparent refractive index gradients, but this has only been observed in one boule and the source is unknown. Furthermore, viewed under a polarizing microscope YLF boules have exhibited none to very few low angle grain boundaries. This is the result of careful seeding and growth from a rigorously clean melt. A view through a 7.5 cm of YLF is shown in figure 6.

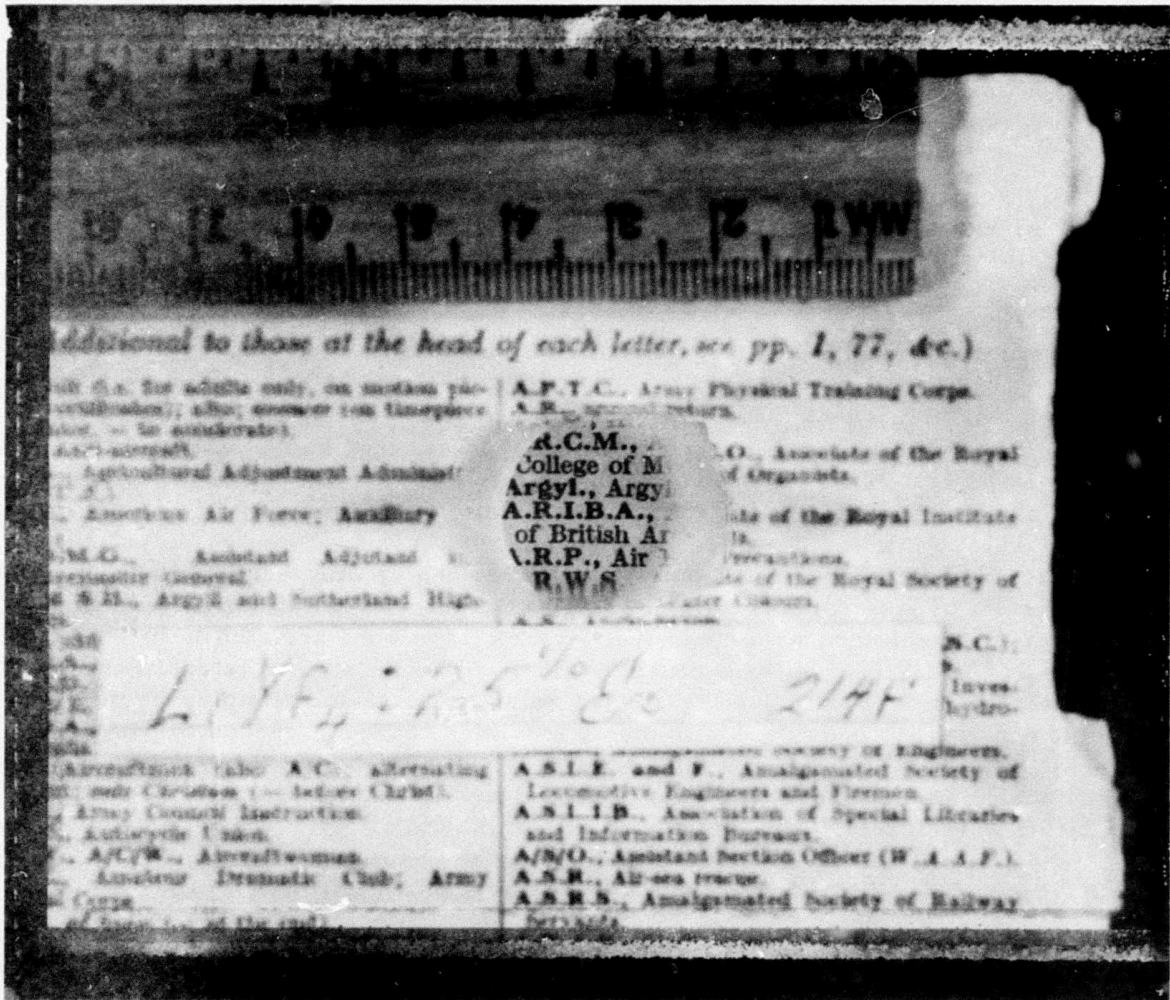
2.3 CRYSTALLINE PURITY

2.3.1 ABSORPTION SPECTRA

IR transmission spectra of a number of samples were recorded to determine whether impurities with absorption peaks in this region are present in detectable concentrations. The results of mass spectrographic analysis indicated (5) very low concentrations of oxygen, OH^- , and Dy^{3+} . Moreover, purification with respect to oxygen and rare earth ions was observed as a result of zone refining, a process now routinely used to prepare feed material.

IR absorption spectra through large optical paths of Er: YLF boules were recorded to determine the presence of trace impurities with absorption in this region. Figures 7 and 8 show spectra of two Er^{3+} boules indicating complete absence of impurities of sufficient concentration to be resolved in this manner.

A further indication of the purity of YLF grown by this technique is provided by the results of laser operation of YLF laser materials. High current density, unfiltered Xe flashlamps with clear fused quartz envelopes are routinely used for pumping Er^{3+} :YLF (4). In experiments with Tb^{3+} YLF, a room temperature laser with emission at $0.55 \mu\text{m}$, dye laser flashlamps are used for pumping (typically 50 joules in $1 \mu\text{s}$) to provide the intense ultraviolet emission needed to pump the material (7). In all the experiments conducted, no evidence of degradation of the optical quality of YLF rods has been observed indicating the complete absence of impurities which are affected by ultraviolet emission.



COPY AVAILABLE TO DDC DOES NOT PERMIT FULLY LEGIBLE PRODUCTION

Figure 6 View Through 7.5 cm of YLF Viewing Direction: Along A Axis.

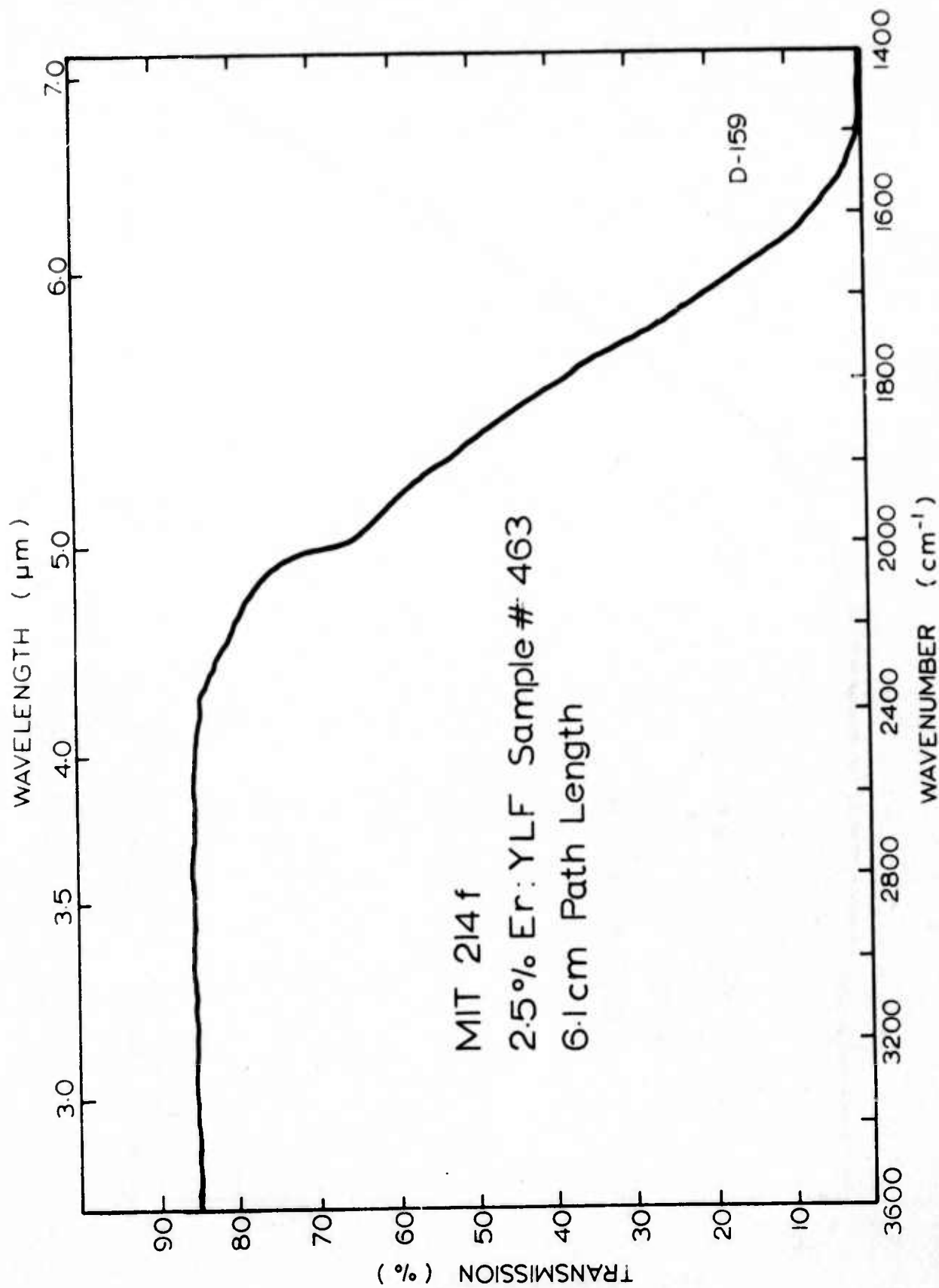


Figure 7 IR Transmission Spectrum of Boule 214f.

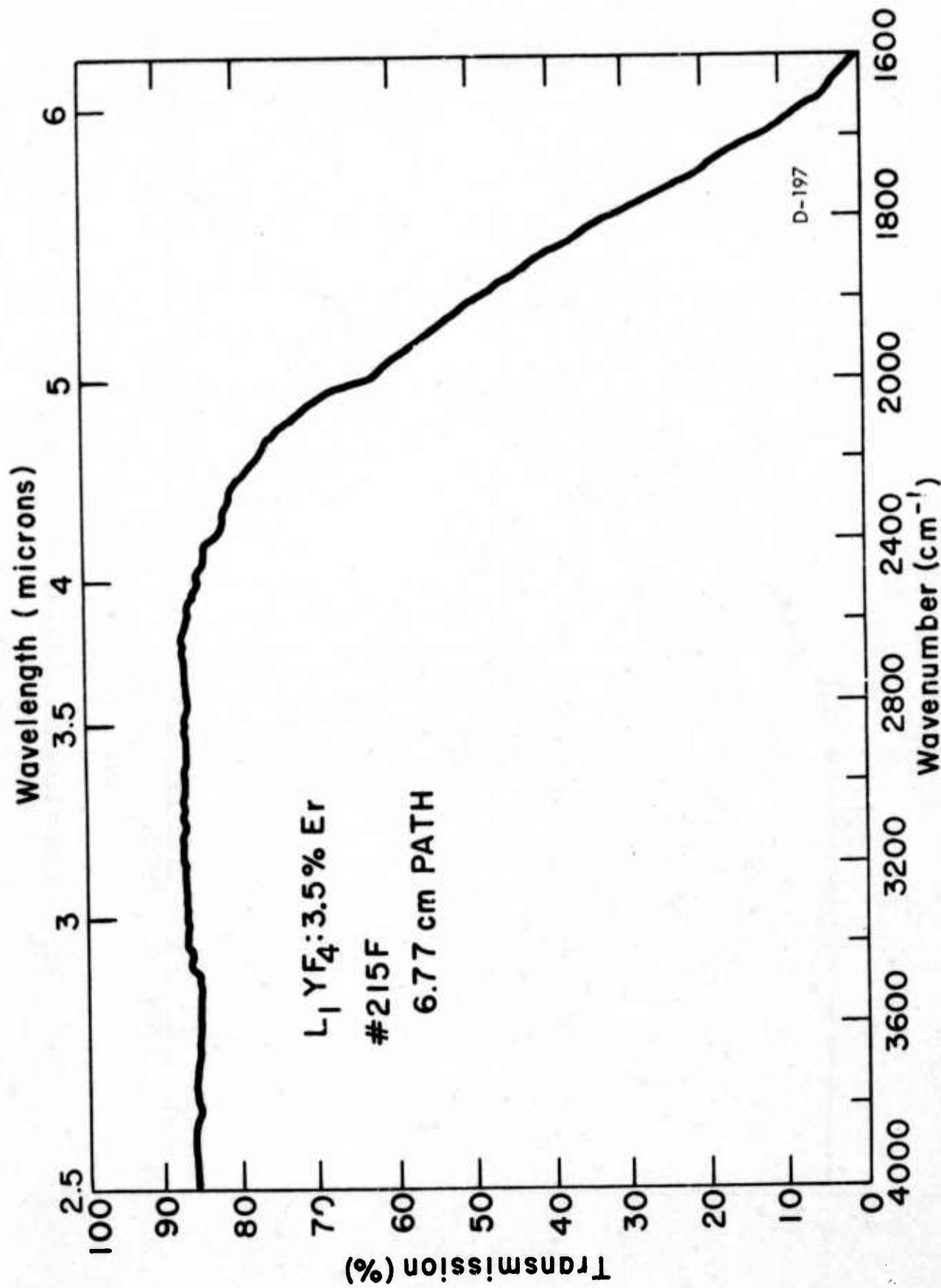


Figure 8 IR Transmission Spectrum of 215f.

2.4 DISCUSSION

There has been much discussion recently about the relationships among optical quality of YLF, feed purity and furnace atmosphere (12, 13). Much of the discussion has centered around the effect of trace oxide and the means of eliminating it. However, the factors affecting crystal quality have not been completely identified. In particular, the nature and composition of light scattering centers is not completely known.

Our approaches to further improve crystalline quality have followed a number of paths. The key areas of investigation have been

- (a) Effects of growth parameters
- (b) Effects of feed purity.

In order to elucidate the chemical and physical nature of inclusions a program of scanning electron microscope analysis (SEM) has been adopted. We have also gained some insight into the effects of oxide on LiYF₄ growth through both deliberate and accidental additions of Y₂O₃ in the melt.

2.4.1 EFFECTS OF GROWTH PARAMETERS

The interrelationship between all the growth parameters is complex. The specific parameters which are known to affect crystalline quality are

- (a) Furnace gas
- (b) Pulling and rotation rate
- (c) Thermal profile of the furnace and temperature stability of the melt.

2.4.1.1 FURNACE GAS

Choice of a furnace gas is limited to inert (He, Ar) or active (HF) atmospheres. The choice of furnace atmosphere is a subject still under active discussion and investigation. Workers at Hughes Research Laboratory have grown various rare earth fluoride compounds in a dynamic HF atmosphere. They evaluate the optical quality of their crystals thusly: "The perfection on a more microscopic level was studied qualitatively by scattering experiments comparing the 90° scattering of several oxide and fluoride materials in an argon laser beam. The Rayleigh or Tyndall scattering was not unusually large . . ." (14).

More recently, a group at Airtron has grown LiYF₄ in a dynamic HF-He atmosphere. (13) Their results are inconclusive. Only one of their reported runs yielded a small haze-free crystal. No indication of the source of inspection light is given; thus it is not possible for the reader to accurately judge the quality of this boule. The presence of HF atmosphere in the furnace did not eliminate the oxide-related problems in their other runs.

Crystal growth in this laboratory had been carried out in a static atmosphere of purified He and is now done in commercial high purity Ar. A significant improvement in crystal quality was experienced when the use of Ar was introduced. The occurrence of isolated bubble type inclusions decreased markedly and the formation in the growth plane of bands of bubbles no longer takes place. We attribute this change in behavior to the decreased solubility in the melt of Ar relative to He. The mechanism of bubble formation using He is believed to be related to exsolved bubbles from the melt nucleating on an impurity site or other melt disturbance at the crystal/melt interface.

2.4.1.2 PULLING AND ROTATION RATES

The effect of pulling (growth) rates ranging from 0.5 to about 5 mm/hr have been tested in growth of $\text{LiYF}_4:\text{Er}$ and other LiYF_4 type materials. At 5 mm/hr boule quality deteriorates markedly and is frequently characterized by extensive formation of nuclei. Over the 2 to 0.5 mm/hr range growth of bubble and striation free crystals has been repeatedly achieved in Ar. There is same indication that growth at 1.5 mm/hr results in better optical quality than growth at a lower rate due to the shorter length of time the crystal spends near its melting point. In other words an annealing effect may be operative which allows more extensive formation of scattering centers at the lower growth rates. Therefore pull rates have been increased to 1.5 mm/hr from the previously used 1 mm/hr to optimize crystal quality.

Crystals are rotated about the growth direction during the whole pulling operation. Although we have not yet investigated this parameter in a systematic way, the following observations have been made.

Rapid changes in rotation rate, especially reductions, result in inclusion formation over the whole growing interface. This effect, when observed, occurs over an interval of a few minutes and is undoubtedly due to a concomitant rapid change in the steady state concentration and temperature profiles at the growing interface.

The diameter of the growing boule is also a function of rotation rate. As in the above case, the effect is probably due to changes in temperature and concentration profile.

Aside from these observations, a systematic investigation of the effect of rotation rate on crystal quality has not been carried out.

2.4.1.3 THERMAL EFFECTS

The thermal profile in the crystal growth furnace has not yet been examined in detail. The importance of this parameter lies in its effects on the shape of the crystal-melt interface and on the rate at which heat can be withdrawn from the

system. Ideally, the interface should be flat if strain-free growth is to be realized. In practice a flat or slightly convex surface is desirable. Also in practice, the major effect of a concave toward the melt interface is not to produce strain but to inhibit mixing in the melt leading to severe inclusion formation. Some changes in radiation shielding in the furnace have been made which help to retain a flat interface during growth. However, accurate thermal studies in the furnace remain to be done.

2.4.2 FEED PURITY

The relationship between YLF crystal quality and melt purity remains largely uninvestigated. Phase diagrams for the systems YF_3 - Y_2O_3 , YF_3 -LiF- Y_2O_3 , YF_3 -LiF- $Y(OH)_3$ are not known. Interactions in solid fluorides between oxygen species and impurity cation species have been studied in some systems (15) but not in $LiYF_4$. It is known that oxygen has a deleterious effect on the quality of YLF crystals but one can only speculate as to why. For example, an oxide bearing phase could precipitate directly from the liquid phase during growth, or it could form afterwards, but at higher temperature by a reaction in the solid phase. Direct formation from the liquid phase could be an equilibrium process or could occur when concentration gradients in the liquid phase lead to local excursions into the oxyfluoride phase field.

Experiments aimed at illustrating answers to some of these questions have been done. To review previous results, crystals grown from zone refined YF_3 have been of better quality than crystals grown from non-zone-refined feed. Details of zone refining were discussed in a previous report.⁽⁵⁾ Crystals #177F and #178F, studied in earlier phases of this program, were grown from zone-refined $LiYF_4$ in contrast to the usual feed which used Harshaw LiF crystal chips. Even though grown in He, these crystals appeared decidedly better than others. A recent growth run of $LiYF_4$ for seed stock used single crystal chips (random cuttings) from previous $LiYF_4$ crystals which had been grown from zone-refined YF_3 . This crystal, #222F, showed no scattering under He-Ne laser illumination. It is not certain, however, whether the purification step involving recrystallization of $LiYF_4$ has been beneficial because impurities introduced in the Harshaw LiF were removed or whether impurities in the YF_3 are more easily removed by recrystallization when LiF is present in the melt. Pursuant to the above results, the techniques for zone-refining of $LiYF_4$ are now being improved.

Oxide segregation during zone refining was discussed in another report.⁽⁵⁾ Additional evidence of oxide segregation in $LiYF_4$ was obtained from a normal freezing experiment done at 0.6 cm/hour in Ar in the zone refiner. The composition $LiYF_4$: 0.167 mole % Y_2O_3 (5000 ppm atomic oxygen) was studied. Starting

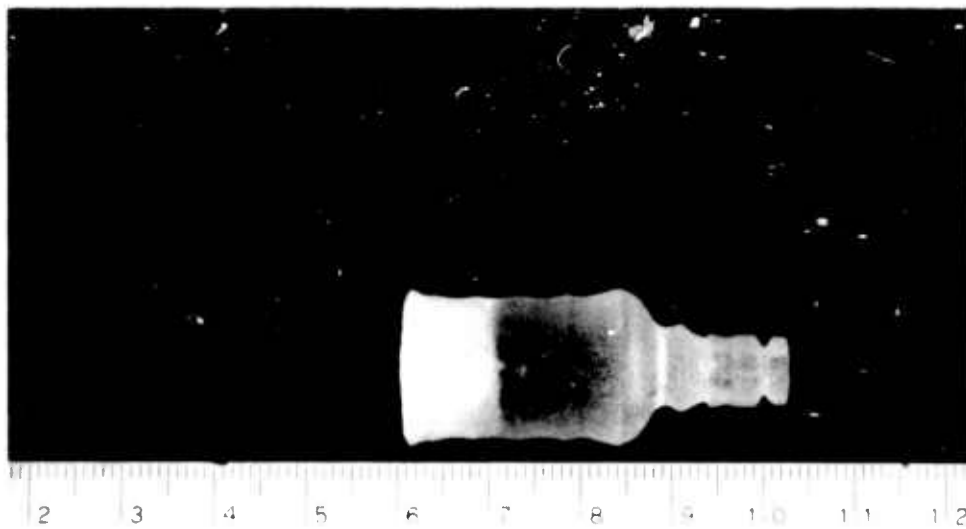
materials were LiYF_4 single crystal chips grown from zone-refined YF_3 and Harshaw LiF , and Research Chemicals 99.99% Y_2O_3 . The first portion of solid that froze was a mixture of YF_3 and LiYF_4 . This was followed, past a sharp boundary, by a clear, haze-free section of sub-cm grains of LiYF_4 , comparable in optical quality to LiYF_4 . The end third, separated from the clear section by a sharp boundary, was a mixture of LiYF_4 and oxyfluoride. The extreme end of the charge which should contain LiF as well was not examined. All phases were identified by X-ray powder pattern analyses. The major oxyfluoride reflection at $d \sim 3.1 \text{ \AA}$ is also found in LiYF_4 that has been oxidized in air above 600°C . Other oxyfluoride reflections are either buried in the noise or overlap LiYF_4 reflections.

Additional corroborating evidence was obtained during the growth of an $\alpha\beta$ YLF crystal, boule 199f, for another program. (16) This crystal was grown from zone-refined LiREF_4 compounds. The LiYF_4 was suspect and an X-ray powder pattern of this material had this extra line at $d = 3.1 \text{ \AA}$, corresponding to an intense reflection of YOF. Nevertheless, a crystal was grown using the contaminated LiYF_4 . A small crystal, shown in figure 9, was obtained which had a very sharp boundary between a clear, almost scatter-free, top section (first part grown) and an opaque section. In fact the scattering was less than is commonly observed in other YLF crystals grown in this and in other laboratories. The effect was observed during the growth run and could be reproduced by partly melting back and re-growing the crystal. This sharp boundary is indicative of passing from a composition region where one solid phase is in equilibrium with the melt. The two-phase region is encountered as the oxide content of the melt increases due to rejection of this species from the growing crystal. An X-ray powder pattern of the bottom, opaque part of the crystal has the extra line at $d = 3.1 \text{ \AA}$. The powder pattern of the clear top is normal. These results indicate:

1. Oxide is rejected from LiYF_4 as it crystallizes.
2. The presence of oxide in the melt does not preclude the possibility that a clear, nearly scatter-free, crystal can be grown.
3. The relationship between trace amounts of oxide in the melt and optical scattering is not simple.

To complement the purification work a program of scanning electron microscopy (SEM) was begun. The purpose of this study was to identify inclusions in Er:YLF by visual and X-ray analyses; chemical methods for removal of impurity elements found at inclusion sites would then be developed.

Samples were taken from the end of 2% Er a laser rod obtained from crystal #180F. The samples were prepared by mechanical polishing followed by argon in milling to expose a clean, undamaged (by polishing) surface. Investigation by SEM followed. The whole surface of the specimen was examined at various magnifications up to 10^4 ; photographs were made and X-ray emission spectra were obtained



199f

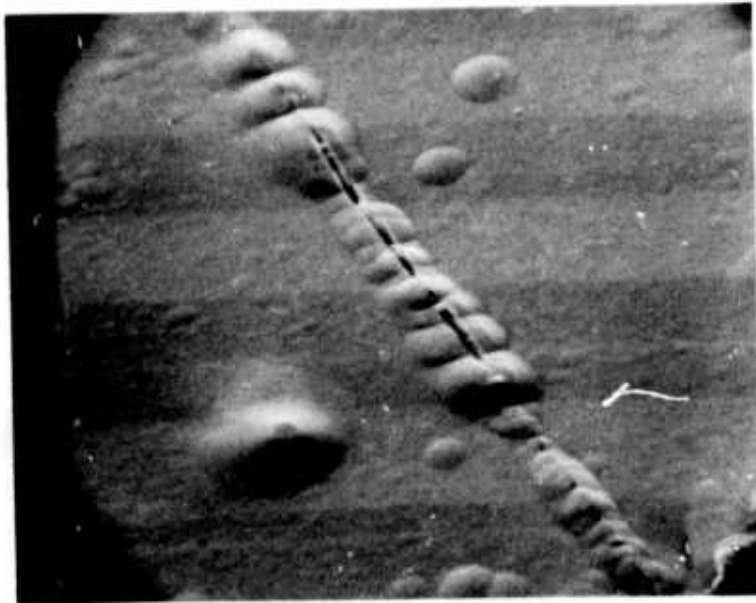
D-214

Figure 9 Boule 199f.

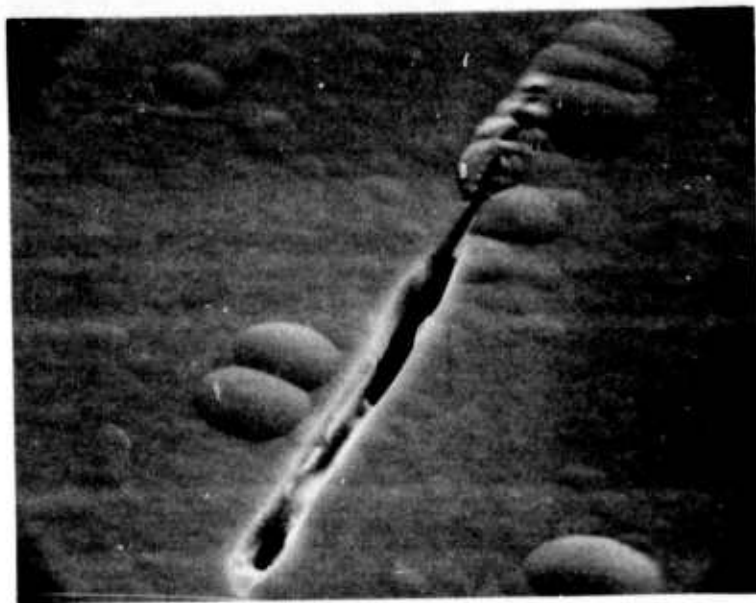
from features suspected of being inclusions. The cycle of ion-milling - SEM inspection was repeated several times exposing successive layers of the sample. Figure 10 shows an elongated bubble exposed by ion-milling. Figure 11 is a portion of the same bubble at higher magnification. Small hillocks are the other prominent surface feature.

Careful examination at magnifications up to 10^4 of ion-milled and freshly fractured surfaces of 180F and various other YLF samples has indicated complete agreement between optical and scanning electron microscopy in characterizing an inclusion as a bubble. What optical microscopy does not reveal is the nature of the bubble's interior. The remaining light scattering centers could not be characterized as bubbles by either technique. Evidence of a well defined crystalline inclusion phase in 180F and other YLF samples, has not been found. X-ray emission spectra from surface features seen on SEM photographs have not shown the presence of localized impurity concentrations. This does not rule out the possibility that impurities other than oxygen are in part responsible for scattering because we are by no means sure that those areas to which X-ray analysis was applied are indeed inclusions.

To continue this work, YLF samples should be investigated in various crystallographic orientations after ion-milling at varying ion energies, in order to better characterize the light scattering centers.



420X



2200X

Figure 10 SEM Photo of Boule 180f.



M = 11200

Figure 11 SEM Photo of 180f.

3.0 PHYSICAL PROPERTIES

In this section we review the physical properties of YLF which have been measured in this and other⁽⁵⁾ programs. The results of these measurements summarized in table I are then applied to the calculation of the thermal load at fracture of a uniformly heated YLF rod cooled only at the surface. A maximum thermal loading of 11 watts/cm is calculated. Based on spectroscopic considerations 7.6 watts/cm output is predicted at this thermal load input in flashlamp pumped operation.

3.1 THERMAL CONDUCTIVITY

The thermal conductivity of a 2% Er:YLF sample was measured by an axial flow technique. The measured value along the a axis of the material was 0.06 W/cm-°K. By contrast the measured values of other laser materials are: SOAP: 0.019, YAG: 0.13, glass: 0.01, W/cm-°K. Thus YLF has a moderately high thermal conductivity. Furthermore because YLF is uniaxial (laser emission is π polarized) the effects of thermally induced birefringence will not be as severe as in the cases of cubic materials. That is, because the laser emission is strongly polarized, losses due to thermally induced birefringence in repetitively pulsed Q-switched operation are expected to be very small.

3.2 MODULUS OF ELASTICITY, RUPTURE AND POISSON'S RATIO

Using strain gage techniques the value of Young's Modulus for YLF was found to be 7.5×10^{11} dynes/cm²⁽⁴⁾ compared to 33×10^{11} for YAG and 17.5×10^{11} for SOAP⁽¹⁷⁾. The modulus of rupture of YLF measured⁽¹⁶⁾ on four samples was found to be 3.3×10^8 dynes/cm². Because this measurement is sensitive to surface imperfections the surfaces of the samples were highly polished. Poisson's ratio, measured in the same apparatus used for the Young's Modulus measurement, was found to be 0.33.

3.3 THERMAL EXPANSION

The thermal expansion of YLF was measured along the two axes of YLF from -196 to 400°C using a recording dilatometer. The results are reported in

TABLE I
MATERIAL AND OPTICAL PROPERTIES

YLF (Li YF_4)

and

YAG ($\text{Y}_3\text{Al}_5\text{O}_{12}$)

<u>MECHANICAL</u>	<u>YLF</u>	<u>YAG</u>
Density (gm/cm^3)	3.99 (undoped)	4.47
Hardness (Moh)	4-5	8.5
Elastic Modulus (dynes/cm^2)	7.5×10^{11}	33.3×10^{11}
Strength (dynes/cm^2)	3.3×10^8	
<u>THERMAL (300°K)</u>		
Thermal Conductivity ($\text{W/cm} \cdot ^\circ\text{K}$)	0.06	0.13
Thermal Expansion Coefficient - ($^\circ\text{C}^{-1}$)	a axis : 13×10^{-6} c axis : 8×10^{-6}	6.9×10^{-6}
<u>OPTICAL</u>		
Index of Refraction $\lambda = 0.6 \mu\text{m}$	$n_o = 1.443$ $n_e = 1.464$	1.8347
UV Absorption	$< 0.2 \mu\text{m}$	$\sim 0.38 \mu\text{m}$
<u>CRYSTALLINE STRUCTURE</u>	Tetragonal (Scheelite)	Cubic (Garnet)

PART I⁽⁴⁾ of this program. At room temperature the values of the thermal expansion coefficients for YLF along the a and c axes are, respectively, 13×10^{-6} and $8 \times 10^{-6} \text{ } ^\circ\text{C}^{-1}$. In contrast YAG exhibits an expansion coefficient of $6.9 \times 10^{-6} \text{ } ^\circ\text{C}^{-1}$ and the reported values for SOAP⁽¹⁷⁾ are 8.9×10^{-6} and $6.6 \times 10^{-6} \text{ } ^\circ\text{C}^{-1}$ along the a and c axes, respectively.

3.4 HARDNESS

The hardness of YLF was measured using a Knoop indenter using a standard load of 50 gms. The measured Knoop hardness was found to be⁽⁵⁾ 260 - 325 kg/mm², independent of orientation. This corresponds to a Moh hardness between 4 - 5 indicating that YLF is relatively soft. The values for YAG and SOAP are 8.5 and 7.0⁽¹⁸⁾ Moh, respectively.

3.5 DENSITY AND LATTICE SIZE

YLF crystallizes in the Scheelite structure with a c/a ratio of 2.08. Values for the unit cell are a = 5.167Å and c = 10.735Å. The density of 2% Er:YLF is 4.03 gm/cm³, that of undoped YLF is 3.99 gm/cm³.

3.6 OPTICAL PROPERTIES

The indices of refraction along the principal axes of YLF, extrapolated from Shand's data⁽¹⁹⁾, are

$$n_o = 1.4405 \quad \text{a axis}$$

$$n_e = 1.4605 \quad \text{c axis}$$

at $\lambda = 0.85 \text{ } \mu\text{m}$. The ultraviolet absorption edge of YLF lies in the vacuum ultraviolet. Preliminary absorption data obtained from reference (20) are presented in table II below.

TABLE II
ULTRAVIOLET ABSORPTION EDGE OF YLF

λ (μm)	a (cm^{-1})
0.1550	2.8
0.1458	4.
0.1379	5.7
0.1305	8.
0.1240	12.
0.1181	22.

3.7 ESTIMATED POWER LOADING AT FRACTURE

The ultimate limitation on the amount of power which can be extracted from a solid state laser material is determined by the heat load for which the rod will fracture. The maximum heat load of a material can be readily calculated based in an analysis due to Henningsen⁽¹⁷⁾ if we adopt the following assumptions:

- (a) The rod is heated uniformly and cooled at the surface
- (b) The rod is isotropic.

YLF, however, is not isotropic so we adopt the "worst case" of assuming the highest thermal expansion coefficient (a axis). The error in this approximation is small compared to that of predicting the laser output per watt of heat input, discussed below.

From (a) and (b) the temperature distribution is obtained⁽¹⁷⁾.

$$T(r) = \frac{1}{4k} Q(r_o^2 - r^2) \quad (3-1)$$

where:

$T(r)$ = temperature at distance r from the axis

r_o = rod radius

k = thermal conductivity

Q = heat/volume dissipated in the rod

This temperature gradient is accompanied by a stress distribution given by⁽¹⁷⁾:

$$\begin{aligned} \sigma_r(r) &= \frac{2\alpha E}{16(1-\mu)k} Q(r^2 - r_o^2) \\ \sigma_\theta(r) &= \frac{2\alpha E}{16(1-\mu)k} Q(3r^2 - r_o^2) \end{aligned} \quad (3-2)$$

and

$$\sigma_z(r) = \frac{2\alpha E}{16(1-\mu)k} Q(4r^2 - 2r_o^2)$$

where:

$\sigma_r(r)$ = radial stress at distance r

$\sigma_\theta(r)$ = tangential stress at distance r

$\sigma_z(r)$ = axial stress (stress parallel to rod axis) at distance r

E = Young's modulus

μ = Poisson's ratio

α = thermal expansion coefficient

From these relations, it is seen that the radial component of the stress vanishes at the rod surface, but the tangential and axial components do not. Thus the rod surface is under tension; at a certain heat load the tension at the surface will exceed the tensile strength of the material causing the rod to crack⁽¹⁷⁾.

At the rod surface ($r = r_0$) the net stress is given by:

$$\sigma_n = \frac{\sqrt{2E\alpha}}{4\pi k(1-\mu)} Q \quad (3-3)$$

Rod fracture will occur at the Q for which σ_n equals the tensile strength of the material (defined as σ). Noting that $P = QA_n$, where P is the input power dissipated as heat and A is the rod cross-section, we obtain the condition for rod fracture at $r = r_0$:

$$\sigma = \frac{\sqrt{2\alpha E}}{4\pi k(1-\mu)} \frac{P}{l} \quad (3-4)$$

That is, rod fracture due to the thermal gradient produced by surface cooling depends only on Young's modulus, the power/unit length, thermal conductivity, Poisson's ratio thermal expansion coefficient, and the tensile strength, but is independent of rod cross-section and the surface temperature.

Rearranging, we can compute the power loading/length at which the material will fracture:

$$\frac{P}{l} = \frac{4\pi k(1-\mu) \sigma}{\sqrt{2\alpha E}}$$

Using the measured values of k , E , μ , α (along the x axis) and σ as shown in table III, we obtain:

$$\frac{P}{l} = 11 \text{ watts/cm for YLF}$$

compared to:

$$\frac{P}{l} = 60 \text{ watts/cm for YAG}$$

Note that the result for YAG is in considerable disagreement with the 150 watts/cm calculated in reference⁽¹⁷⁾, although the same analysis was applied.

We must now estimate the amount of heat per watt of laser output generated in the material. In a "properly designed system" 1.5 watts of heat/watt of laser output in Nd:YAG is reported in reference (17). The energy decrement between the useful pump bands and the upper laser level in Er^{3+} :YLF is considerably less than in Nd:YAG. Furthermore, the multiphonon relaxation rates are nearly an order of magnitude lower in YLF, and pump radiation in the regions of direct lattice absorption ($6 \mu\text{m} < \lambda < 0.15 \mu\text{m}$) can easily be filtered. Therefore, we adopt the 1.5 watts of heat/watt of laser output as a conservative approximation and obtain as the maximum output power/cm:

$$\frac{P_{\text{out}}}{l} = 7.6 \text{ output watts/cm at thermal fracture}$$

Operating at 0.2 times the maximum thermal loading, we obtain 11 output watts for a 70 mm rod. At this input power level (16 watts) the temperature gradient from the rod center to the surface (from equation 3-1) is only 2.8°C . Note that for Nd:YAG we calculate 60 output watts under the same conditions (70 mm rod at 0.2 times thermal fracture).

It is emphasized that this calculation, based on the assumption of a uniformly heated isotropic rod cooled at the surface, is only approximate as YLF is uniaxial. However, it reveals no fundamental limitation for operation in the 1 - 10 watt range for reasonably sized rods. To what extent other factors may limit the output in this material is not yet clear. In Section 5.0 of this report an average power of 0.8 watts is reported from a 4 cm rod without any evidence of material limitations.

TABLE III
PHYSICAL PROPERTIES OF YLF AND YAG

	YLF	YAG*
Thermal Conductivity, k W/cm - °C(20°C)	a axis: 0.06	0.13
Thermal Expansion Coefficient, α °C ⁻¹	a axis: 13×10^{-6} c axis: 8×10^{-6}	6.9×10^{-6}
Young's Modulus, E dyne/cm ²	7.5×10^{11}	3.3×10^{12}
Poisson's Ratio, μ	0.33	0.3
Tensile Strength, σ dyne/cm ²	3.3×10^8 **	1.7×10^9

* Airtron Data Sheet

** Assumed equal to the Modulus of Rupture

TABLE IV
THERMAL LOADING AT FRACTURE

	YLF*	YAG
Thermal Loading at Fracture P/l (watts/cm)	11	60

* Assumed isotropic with a axis a

(THIS PAGE LEFT INTENTIONALLY BLANK)

4.0 SPECTROSCOPY

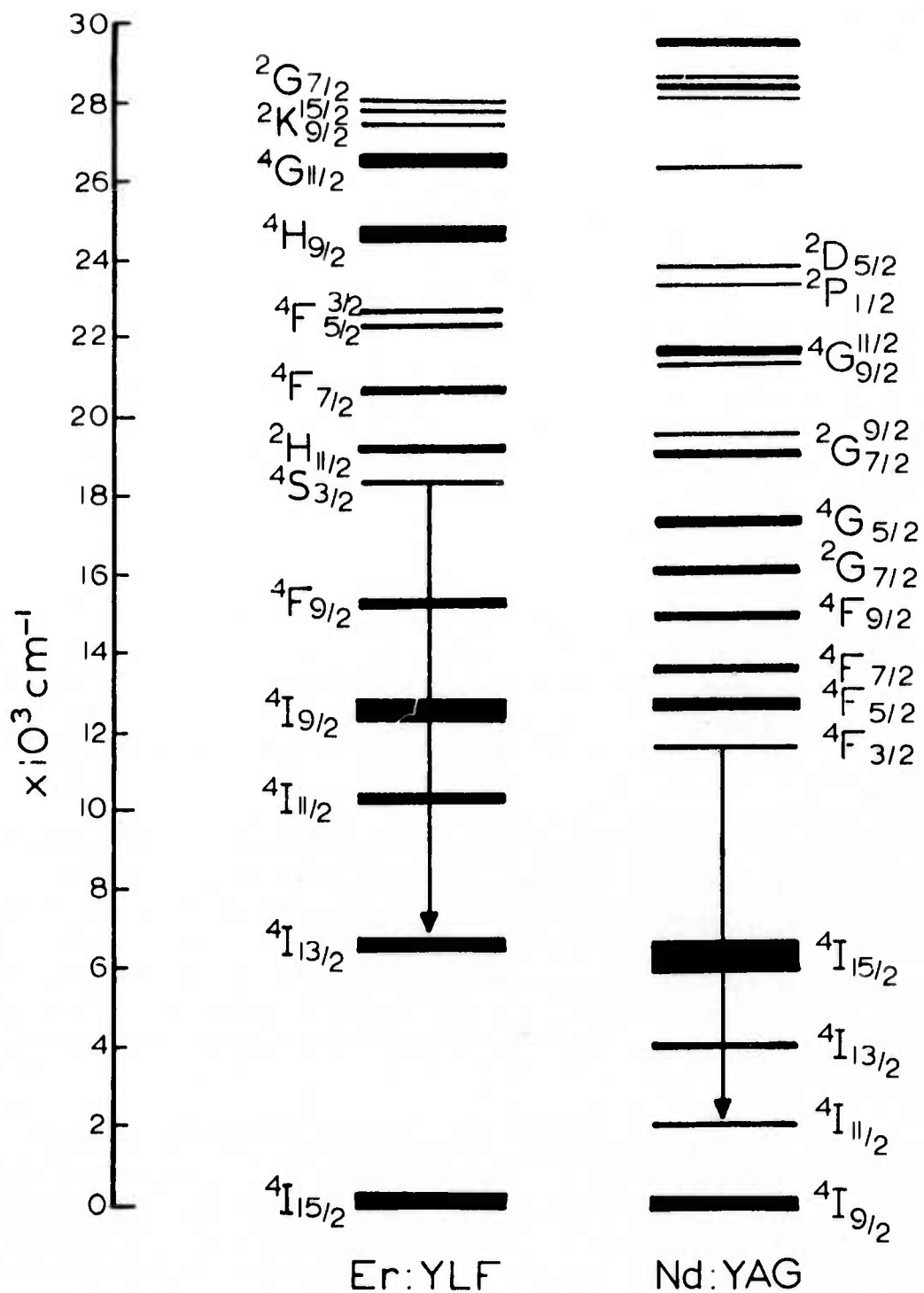
The spectroscopy of Er^{3+} :YLF which pertains to laser operation is fairly straightforward. The pertinent spectroscopic parameter for Er^{3+} :YLF are presented in references 4 and 6. Some of the energy levels of this system are shown in figure 12 together with those for Nd:YAG. The similarities are obvious; both are unsensitized four level lasers⁺ with groups of closely spaced pump bands which feed the upper laser level. A more careful analysis of the similarities and differences of these systems and some of the implications thereof are discussed in Section 6.0 of this report.

One very significant difference between these systems is that in Er^{3+} :YLF the terminal manifold is very long lived (~13ms). The implications of this were analyzed in a previous report.⁽⁶⁾ Contrary to the conclusions of reference 22, it was determined that provided direct pumping of $^4I_{13/2}$ is avoided the effect of the long terminal manifold lifetime on the extractable energy in single shot operation is negligible.

However in repetitively pulsed operation at fairly high repetition rates (greater than 20 Hz) the possibility of saturation effects due to buildup of the terminal level population cannot be excluded. To this end it was determined that Pr^{3+} in low concentrations was very effective in quenching the terminal manifold without significantly degrading the upper level storage time.⁽⁶⁾ In the composition 2% Er - 0.5% Pr, for example, the $^4I_{13/2}$ manifold is quenched by more than a factor of 30 ($^4I_{13/2}$ lifetime less than 0.4 ms) and the upper level lifetime is essentially unaffected.

In this section spectroscopic studies directed at improving the laser efficiency are described. Quenching of the upper laser level was investigated as a function of Er^{3+} concentration and temperature. The intent was to improve the pumping efficiency in laser operation by means of increased Er^{3+} concentration. Concentrations from 0.5 to 3.5% Er were investigated; the results indicate that:

⁺ In some special cases the terminal level population cannot be neglected in Nd:YAG (see reference 21).



D-139

Figure 12 Energy Level Diagrams of Er:YLF and Nd:YAG.

- At room temperature the optimum concentration is near 5%.
- Below room temperature very significant improvements in the storage time of the upper laser level can be obtained even with much higher Er^{3+} concentrations.

4.1 CONCENTRATION QUENCHING

The time dependence of the $^4\text{S}_3/2$ fluorescence amplitude at room temperature for five different Er^{3+} concentrations is shown in figure 13 together with the calculated decay constants (lifetimes). Samples were irradiated with a short flash (20 μs total duration, 2 μf , 2 KV) from an EGG FX33-1.5 flashlamp appropriately filtered (1 cm CuSO_4 , 2 Corning CS7-37 filters). The fluorescence was filtered with two .85 μm band pass filters and detected with an S-1 PMT. The output of the PMT, across 1 K ohm, was displayed on a Tektronix 545 scope and photographed. The uncertainties in the lifetimes tabulated reflect possible uncertainties in the value of the points due to the signal/noise ratio of the data.

These data require some explanation as the $^4\text{S}_3/2$ lifetime in Er:YLF cannot be characterized by a single exponential, at least for two of these concentrations at room temperature. Instead an initial rapid decay followed by a slower decay is observed in some samples. In figure 13 the plots of the \ln (fluorescence amplitude) vs time for the 2% Er and 2.5% Er samples are not linear. This results in considerable ambiguity in the calculated lifetime for these two concentrations. For example, if the initial 100 μs of data are neglected (to eliminate artifacts associated with possible slow buildup times of the upper level) then within the reading error discussed above we obtain the following straight line fits:

$$2\% \text{ Er - decay rate: } 268 \pm 20 \mu\text{s}$$

$$2.5\% \text{ Er - decay rate: } 220 \pm 20 \mu\text{s}$$

for the data between $\sim 125 - 600 \mu\text{s}$.

To determine the decay constants for a multiple decay (with two assumed rates) we must fit the data to:

$$y(t) = A \exp(-\alpha t) + B \exp(-\beta t) \quad 4-1$$

where y is the fluorescence amplitude at time t and A , B , α , β are constants and $\beta < \alpha$. In principle B and β can be obtained by noting that (for $\beta < \alpha$)

$$y(t \rightarrow \infty) \sim B \exp(-\beta t)$$

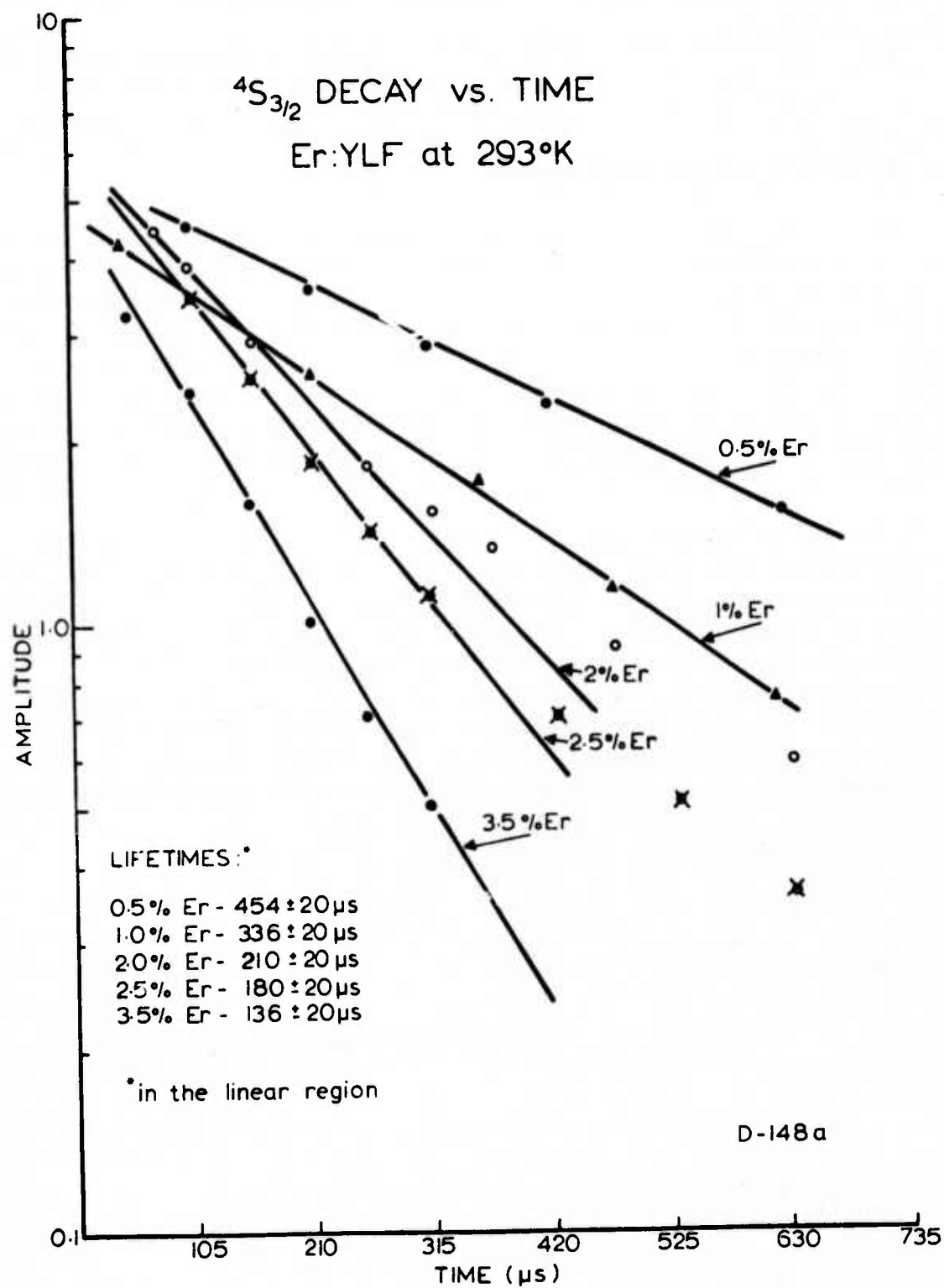


Figure 13 Time Dependence of $^4S_{3/2}$ Decay in Er:YLF.

i. e. the linear portion for times sufficiently long contains only the constants B and β which can be obtained directly from the straight line fit in this region. A and α can then be obtained by fitting 4-1 to the early data. Unfortunately, the uncertainty in the data for $t > \sim 400 \mu\text{s}$ will not allow for utilization of this procedure with reasonable accuracy. For the 2% and 2.5% composition we have neglected the latter portion ($t \sim 200 \mu\text{s}$) of the decay as this is the effective storage time for flash pumped laser operation.

Figure 14 shows a plot of the $^4\text{S}_{3/2}$ decay rate (= inverse fluorescence lifetime) versus Er^{3+} concentration. The curve beyond 3.5% Er is extrapolated and predicts a $100 \mu\text{s}$ lifetime for 5% Er. The question is what is the effect of the increased pumping efficiency and the decreased storage time in laser efficiency.

For the room temperature case an estimate of the "optimum" composition can be obtained using a very simple argument. The rate equations for a simple two level system are:

$$\dot{N}_u = W_{12} N_l - N_u R$$

where N_u (N_l) is the upper (lower) level population density, W_{12} is the pumping rate (proportional to the absorption coefficient \times pump intensity), and R is the decay rate of the upper level. Solving for the simple case of the equilibrium values ($\dot{N} = 0$) we obtain:

$$N_u = \frac{W_{12} N_l}{R}$$

A plot of N/R vs T is shown in figure 14 indicating (from extrapolated values of R) a broad maximum of N/R at $N \sim 5\%$. We note that this is a "worst case" analysis in the sense that in pulsed operation a pump pulse longer than the lifetime was assumed. This is discussed in more detail in Section 6.0 of this report.

4.2 TEMPERATURE DEPENDENCE

The temperature dependence of the $^4\text{S}_{3/2}$ lifetime of a 3.5% Er^{3+} :YLF sample was measured from 77 - 293°K. The sample was mounted in a variable temperature dewar and excited with a $1 \mu\text{s}$ Xe discharge. The output of an S-1 PMT was analyzed in a Computer of Average Transients. The results plotted in figure 15 show a very rapid increase of the $^4\text{S}_{3/2}$ lifetime as the temperature is decreased. For reference the lifetimes of dilute samples reported in reference 23 at 6°K are:

$$0.5\% \text{ Er:YLF} : 600 \pm 30 \mu\text{s}$$

$$2\% \text{ Er:YLF} : 608 \pm 30 \mu\text{s}$$

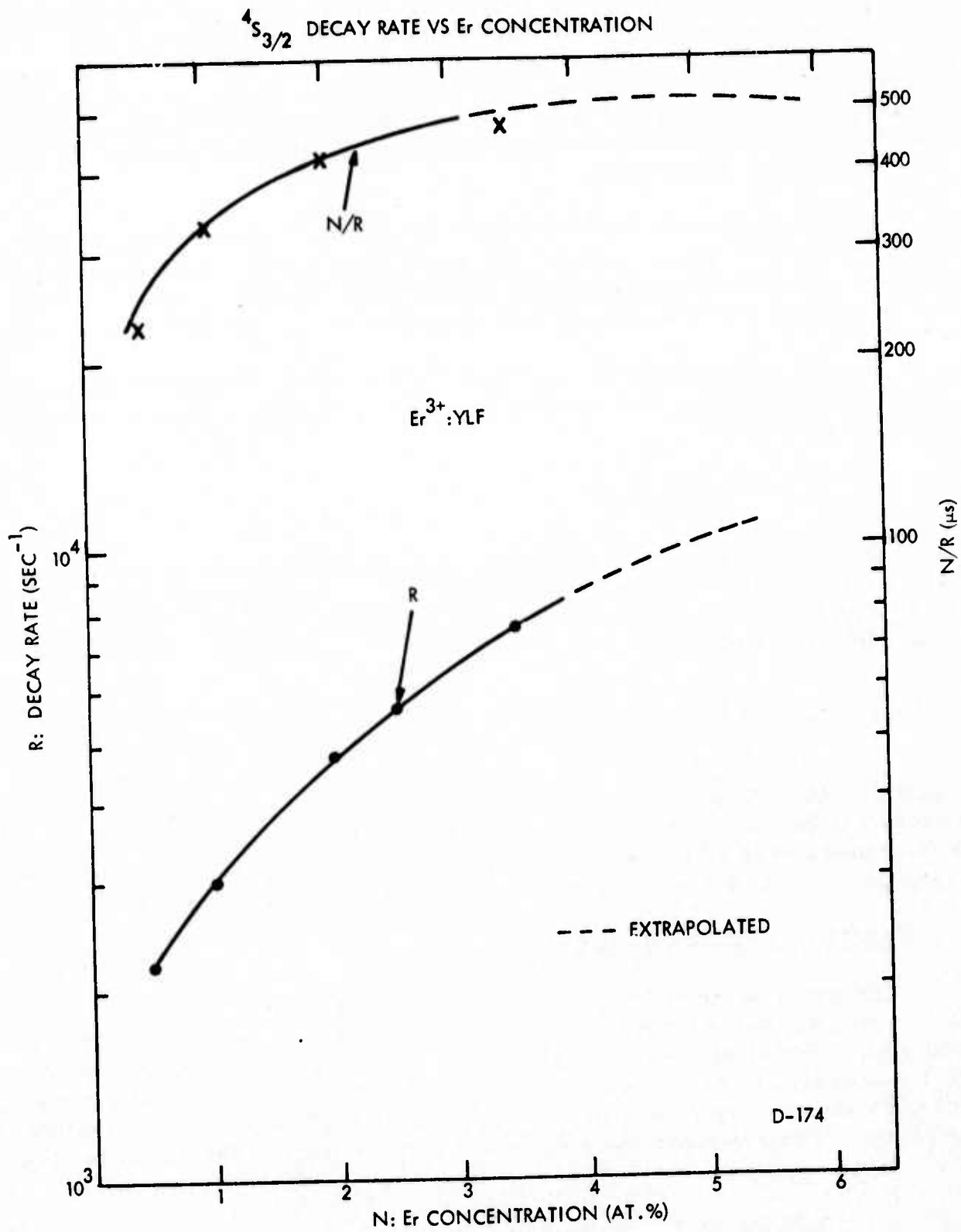


Figure 14 Decay Rate vs Concentration.

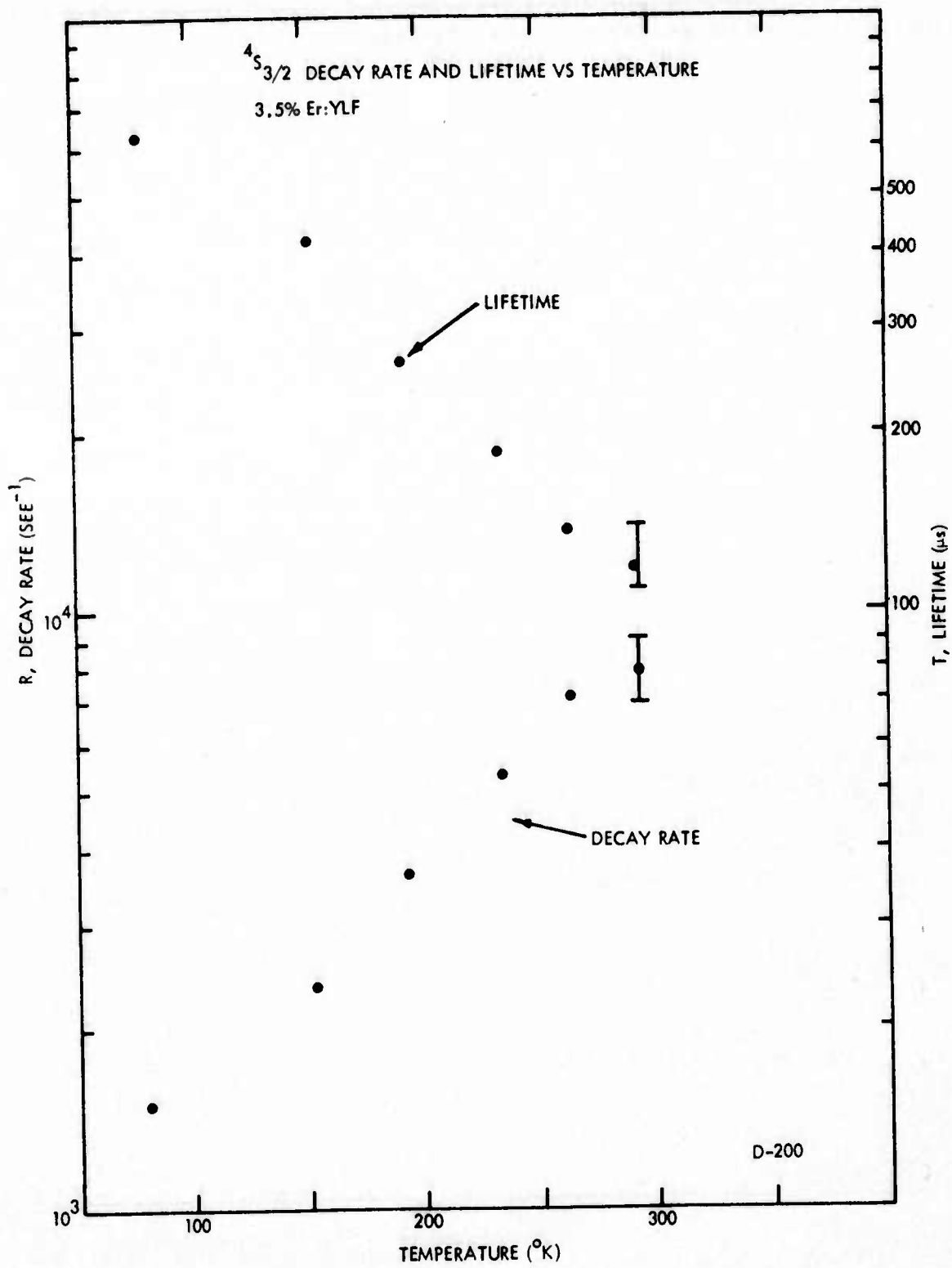


Figure 15 $4S_{3/2}$ Decay Rate and Lifetime vs Temperature.

This indicates that concentration quenching is very weak at low temperatures and very high Er^{3+} concentrations, greater than 10%, may be utilized for very efficient pumping at low temperatures without serious degradation of upper laser level storage time. However high pump band quantum efficiencies as a function of concentration and temperature must be maintained.

5.0 LASER MEASUREMENTS

The focus of laser measurements for this program were:

- determination of the average power capability of Er^{3+} :YLF in flashpumped operation,
- determination of the effects of compositional changes on the laser efficiency,
- determination of the effects, if any, of the long terminal manifold lifetime on laser performance,
- measurement of Q-switched performance.

The key results obtained are summarized below.

- A comparison of long pulse laser performance using rods of varying Er^{3+} concentration showed dramatic improvements in efficiency with concentration over the range 2 - 3.5% Er^{3+} . The slope efficiency of a 3.5% Er rod was found to be twice that of a 2.5% rod of similar quality.
- The improved quality of rods grown in an argon atmosphere was substantiated by laser measurements. Observed efficiency and average power outputs were substantially higher with rods grown in argon.
- The output power vs repetition rate in long pulse operation was measured for a 5.1×41 mm, 2.5% Er^{3+} :YLF rod. At 10 Hz with 630 watts input 0.57 watts output were obtained. Thermal limitations were not encountered at water flow rates of 0.5 gal/min and the output power was observed to correspond to the output energy obtained in single shot operation times the repetition rate.

- Q-switched outputs of only a few millijoules had been obtained to date using calcite/KD*P. Poor Q-switched performance is attributed to losses due to the calcite polarizer. Thermally induced birefringence is ruled out as the material is uniaxial and the "loss" to the polarizer was independent of repetition rate. Q-switched operation using a saturably absorbing dye was obtained on a company sponsored program. Pulsewidths of 50 - 100 ns at FWHM were obtained at 10 Hz operation with an average power of 50 mw.
- The highest output power observed was 0.8 watts at 25 Hz, the highest repetition rate observed was 50 Hz (2.5% Er, 5.1 x 41 mm).

5.1 EFFECTS OF Er³⁺ CONCENTRATION

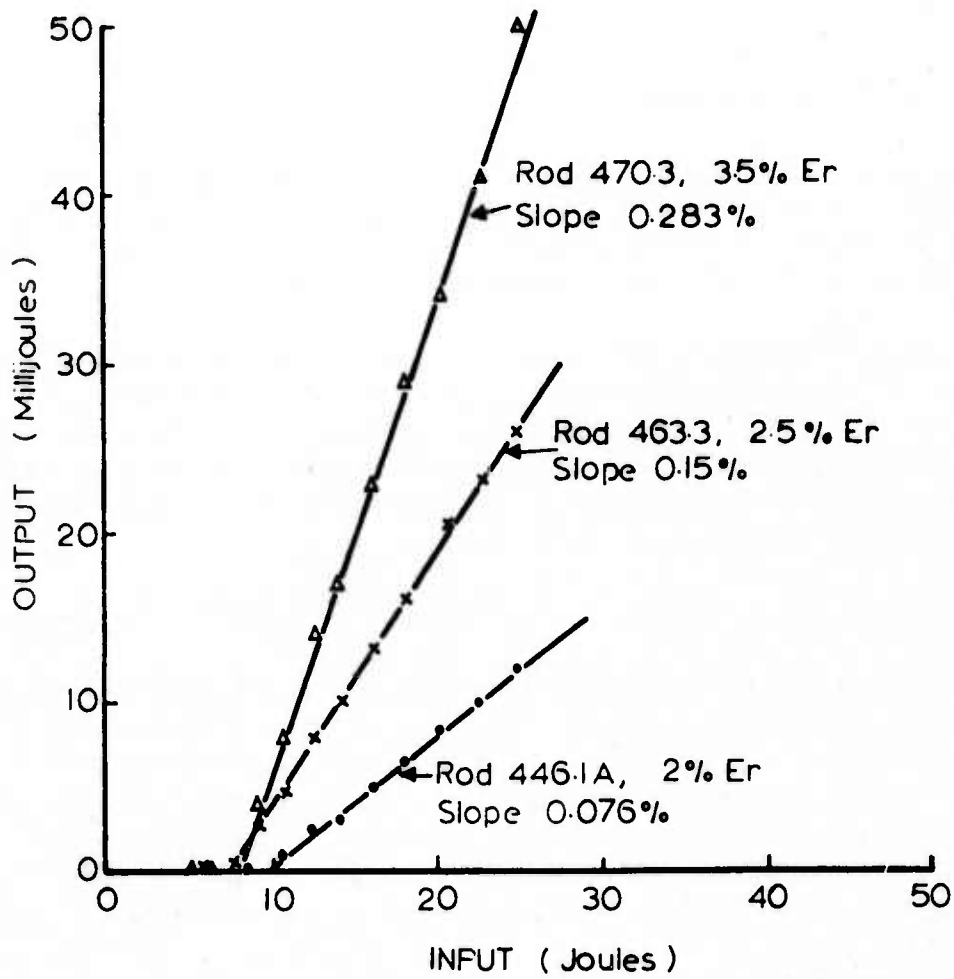
Comparative laser data were taken with rods of three different Er³⁺ concentrations. The experimental conditions were:

Flashlamp:	3 x 30 mm, 1LC 3000 torr Xe
Storage Bank:	50 μ f, 8 μ h
Pump Cavity:	front surface silver, $l = 50$ mm, cylinder cut to elliptical cross section: $a = 0.65$ $b = 0.6$ mm
Resonator:	MAX R - 1 meter radius, 95%R flat, length 24.5 cm
Lamp Pulsewidth:	60 μ s FWHM
Rod Dimensions:	446.1a : 5.5 x 52 mm, 3% Er (180f) 463.3 : 5 x 60 mm, 2.5% Er (214f) 470.3 : 5 x 47 mm, 3.5% Er (215f)

Care was exercised in these experiments to assure that the results were not due to artifacts in mirror alignment or pump efficiency parameters. Unfortunately the rod lengths were not identical and, more significantly, the optical quality of one of the rods, 446.1a, was poor. All the rods were rough ground with uncoated faces.

The results are shown in figure 16. As the optical quality of rods 463.3 and 470.3 (grown in argon) were qualitatively similar, differences in performance can be attributed to the Er³⁺ concentration or the differences in rod length. Note that

Room Temperature
Long Pulse
95% R



D-166

Figure 16 Laser Efficiency vs Er³⁺ Concentration.

the pump conditions employed (30 mm lamp, 50 mm pump cavity) favor shorter rods. We can estimate the relative performance of two identical rods differing only in length by the following. The fraction of resonator energy coupled out per pass is given by (24).

$$f = \frac{1 - R}{1 - R + 1 - \exp(-2l\delta)}$$

5-1

where R is the output mirror reflectivity, l is the rod length, and δ is the loss/cm. We assume $\delta = 0.01 \text{ cm}^{-1}$ for both 470.3 and 463.3 and, using $R = 0.95$, obtain

$$f = 0.34 \text{ for a 50 mm rod}$$

and

$$f = 0.31 \text{ for a 60 mm rod.}$$

Since both rods have the same volume of material pumped (the excess length of the longer rod was shadowed), the effect of the difference in length on the output is given by f . Thus, we conclude that the data reflects the improved long pulse efficiency of the 3.5% Er^{3+} concentration over the 2.5%.

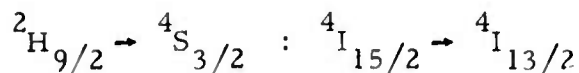
The 2% Er rod (grown in the helium) was of considerably lower optical quality than the other two rods and its behavior compared to the other two rods may not simply be due to the concentration differences. For example, if we assume a scattering loss of 0.03 the fraction coupled out, using equation 5-1, is 0.16 or approximately half that for a rod with $\delta = 0.01$. Unfortunately, quantitative estimates of the scattering losses are not available.

5.1.1 REMARKS

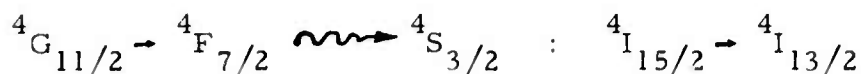
It is tempting based on these results to suggest that further increases in laser efficiency with Er^{3+} concentration. In YLF a very large amount of Er^{3+} can be substituted for the Y^{3+} up to LiErF_4 without affecting the ease of growth or the crystalline quality. Furthermore, the $^4\text{S}_{3/2} \rightarrow ^4\text{I}_{13/2}$ fluorescence linewidth is insensitive to Er^{3+} concentration as the Er^{3+} does not significantly distort the lattice. The only apparent limitation, from spectroscopic considerations, is the quenching of the upper level lifetime at room temperature with increased concentration.

Figure 14 shows the $^4\text{S}_{3/2}$ decay rate (= inverse of the fluorescence lifetime) versus Er^{3+} concentration at room temperature. It is seen that concentration quenching is in evidence even in very dilute crystals. The problem then is the trade-off between increased pumping efficiency and the decreased storage time as the Er^{3+} concentration is increased.

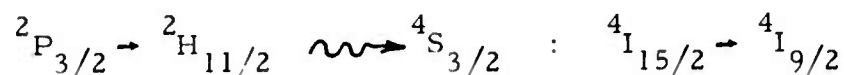
The fundamental constraint is that the pumping rate must be much faster than the decay rate in order to achieve inversion. In low Er^{3+} concentrations the buildup of the upper level ($^4\text{S}_{3/2}$) occurs within $10\mu\text{s}$. As the concentration increases, however, the buildup rate may increase if processes other than multiphonon relaxation are operative. For example a number of ion pair processes are possible which can excite $^4\text{S}_{3/2}$



or



or



The transitions to the left of the colon occur in the initially excited ion; those to the right occur in an ion initially in the ground state. Such processes would exhibit concentration dependent rates so at higher concentrations the buildup times might be considerably faster than $10\mu\text{s}$. Until the rates and modes of relaxation of the $^4\text{S}_{3/2}$ pump bands are determined as a function of Er^{3+} concentration, the fundamental limitation on the Er^{3+} decay rate can only be guessed at. However, the performance of the 3.5% Er^{3+} rod, (lifetime $135\mu\text{s}$) strongly suggests that the pumping rate limitation may not be a limiting factor for Er^{3+} concentrations within the range of extrapolation in figure 14.

Neglecting pump rate limitations due to internal relaxation we identify two regions of operation:

$$T \ll \tau$$

$$T \gtrsim \tau$$

where T is the pump pulsewidth and τ is the fluorescence lifetime. In the first case the actual lifetime is irrelevant provided we maintain the inequality. Once the upper laser level is sufficiently populated the loss to stimulated emission far exceeds that due to fluorescence. However, in practice flashlamp loading constraints prevent arbitrary increase of the Er^{3+} concentration. For example,

for a 4×50 mm 450 torr Xe flashlamp driven by a critically damped $50\mu\text{s}$ pulse the explosion energy is 200 joules. At $10\mu\text{s}$ it is 80 joules. For 10^6 shots we must operate at $0.2 \times$ the explosion energy or 40 and 16 joules respectively. As the lifetime of 3.5% Er:YLF is only $135\mu\text{s}$ maintaining $T \ll \tau$ is impractical at least for systems applications using conventional flashlamps.

Thus we are forced⁺ into the regime where $T \gtrsim \tau$. This condition is considered in Section 4 and an optimum concentration of approximately 5% Er is predicted.

The last point of interest is the relative performance of the 3.5% and 2.5% compositions. Under the ideal conditions, $T \ll \tau$, we would expect the efficiency to scale with active ion concentration. That is, we would predict the threshold to be reduced by a factor of $3.5/2.5 = 1.4$, and the slope efficiency to increase by the same factor. This follows from the assumption that the upper level population density is proportional to the active ion density. However, from figure 16 we see that the threshold is reduced by a factor of only 1.1 and the slope efficiency increased by a factor of 1.8 in the rod of higher Er^{3+} concentration. This indicates that the assumption of pumping efficiency proportional to active ion concentration is inadequate. However, additional increases in the active ion concentration certainly should be attempted in view of the trend of the data.

5.2 REPETITIVELY PULSED OPERATION

Experiments were carried out in a number of different pump cavities to evaluate the average power capabilities of the material. These experiments were not intended as performance comparisons and caution should be exercised in attributing performance variations to nominal changes in operating conditions except where specifically noted.

5.2.1 ROD 463.4:2.5% Er:YLF

The output power vs repetition rate with input energy and water flow rate as parameters was measured. The pump cavity was not optimally efficient; but good mechanical support for the laser rod was provided and no artifacts due to laser rod motion were observed. The experimental setup utilized was as follows:

⁺ The use of dye laser flashlamps should be investigated as an alternate means of pumping in view of the position of the pump bands in this material ($\lambda < 0.55 \mu\text{m}$) and the resistance of YLF to ultraviolet induced damage. In this case high concentrations could be utilized ($> 10\%$) for good pumping efficiency while maintaining $T < \tau$.

Rod:	463.4 (214f) 5.1 × 52 mm 2.5% Er:YLF 41 mm of rod exposed to the flashlamp
Flashlamp:	ILC - 3000 Torr 3 mm × 60 mm
Pulsewidth:	70 μ s FWHM
Pump Cavity:	8 inch diameter aluminized sphere
Resonator:	MAX R (1 meter radius), 70% R (flat) length 70 cm, rod uncoated
Storage Bank:	25 μ f, 23 μ H
Trigger Mode:	Parallel to Cavity
Cooling:	tap water over lamp and rod

The rod (grown in an argon atmosphere) is of relatively high optical quality; inclusions are visible only under high magnification or from scattered radiation of a He-Ne probe beam.

Figure 17 shows the single shot input/output characteristics in long pulse. In figure 18 the output vs input power for different input energies is plotted at a flow rate of 1 gal/min. Power supply limitations prevented operation at 63J/15 Hz. The error bar for the data at 15 Hz reflects the uncertainty in the input energy; at 15 Hz the charging cycle of the power supply is too slow to reach the nominal charging voltage. The charging voltage at 15 Hz was observed on an oscilloscope; the corresponding uncertainty in an input energy ($\pm 5\%$) resulted in an uncertainty of $\sim \pm 4$ mJ in output energy of ± 60 mW in output power at 15 Hz. At 10 and 5 Hz where the supply was capable of charging to the nominal voltage the uncertainty in the data is largely due to the power meter reading error, $\sim \pm 20$ mW.

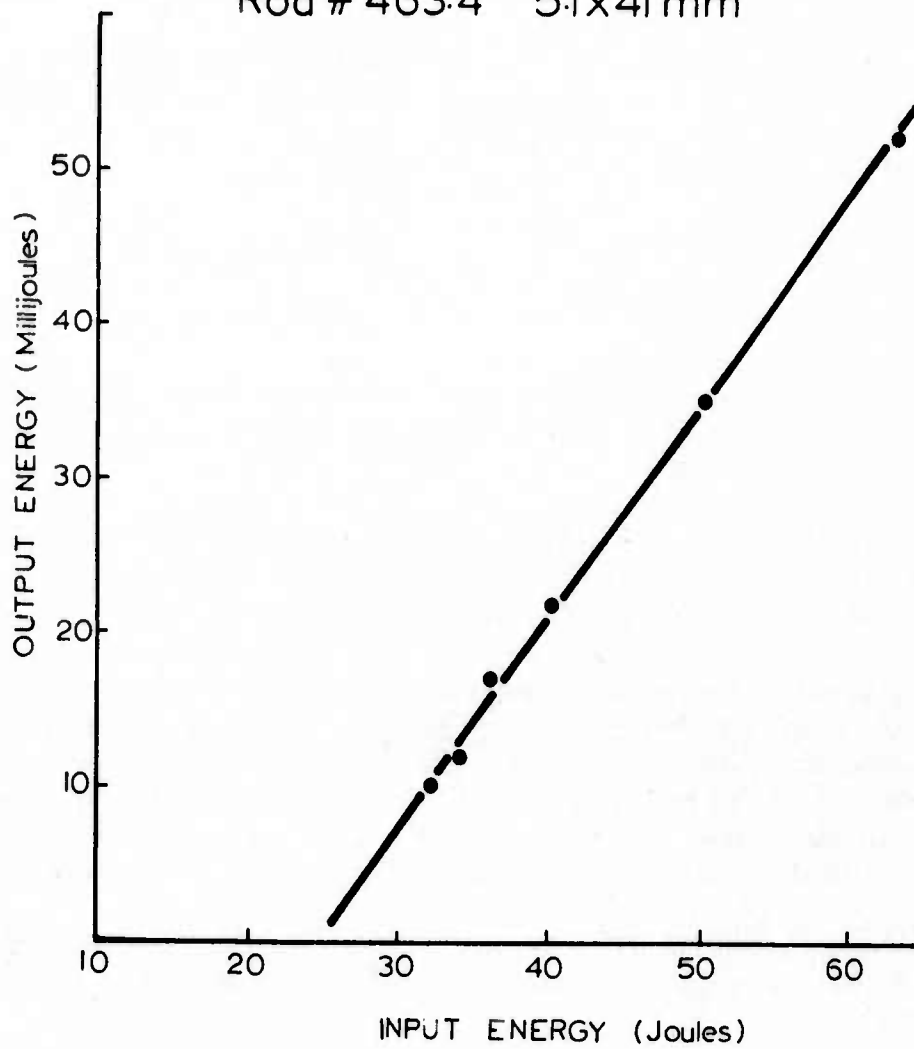
At 0.5 gal/min these results were reproducible to within the experimental error. At 0.1 gal/min the output at 15 Hz fell substantially below the values shown in figure 17.

At 15 Hz 570 mW from an active volume of 0.84 cm³ was obtained in long pulse. Scaling the power output proportional to volume we obtain for 0.25 × 3 inch rod (2.4 cm³) 1.6 watts output long pulse at 15 Hz. Power supply limitations prevented operation at higher loadings. Operation for extended periods (5 min. at 0.5 gal/min at 750 watts input, 570 mW output was obtained.

In other experiments this same rod in a more efficient pump cavity input powers of 2 KW were sustained for brief periods without thermal fracture.

0.85 μ m LONG PULSE INPUT vs. OUTPUT

Single Shot 70%R
Rod # 463.4 5.1x41 mm



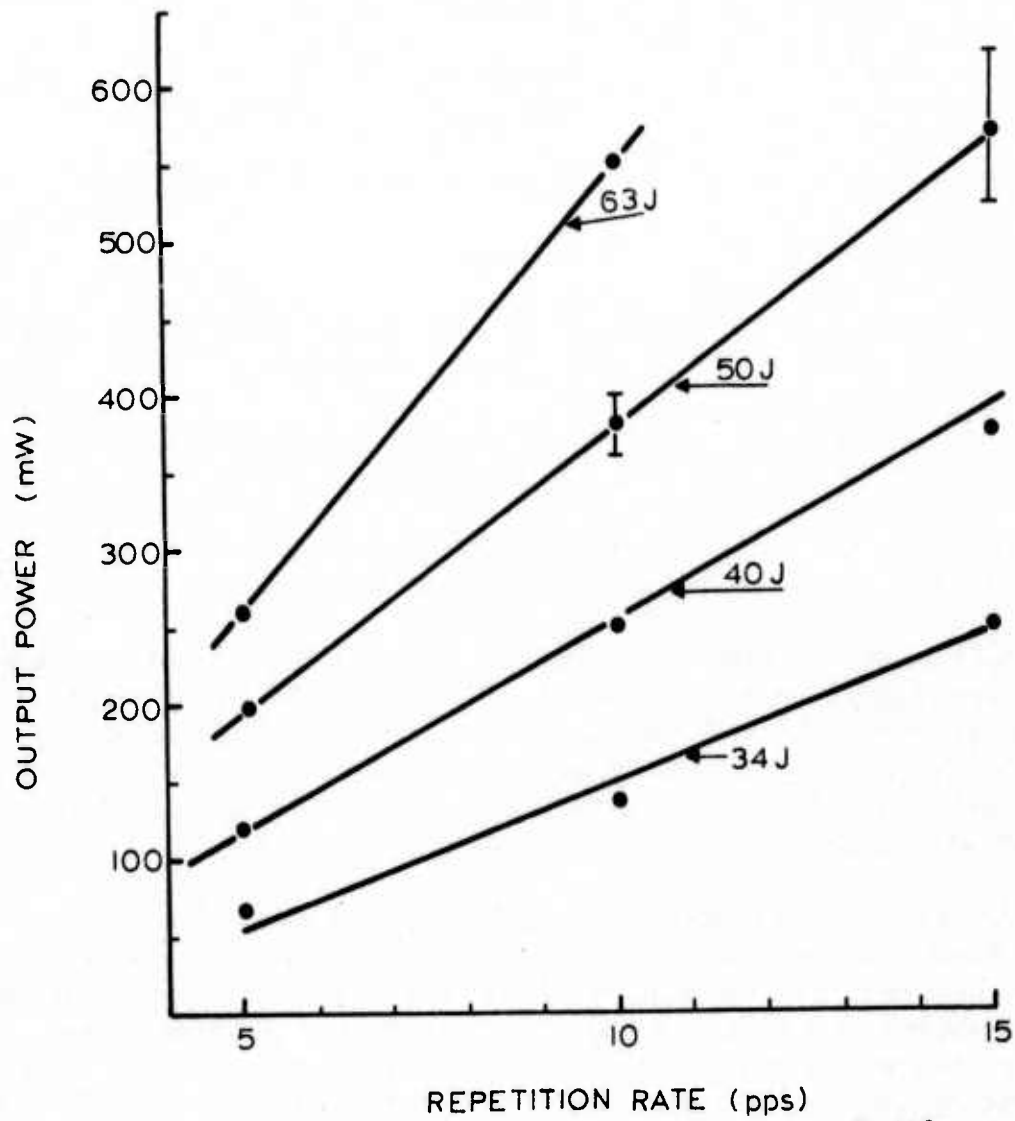
D-147

Figure 17 0.85 μ m Long Pulse Input vs Output.

0.85 μ m LONG PULSE OUTPUT vs. REP. RATE

Rod # 463.4 5.1 x 41 mm

Flow Rate 1.1 gal/min



D-146

Figure 18 0.85 μ m Long Pulse Output vs Rep. Rate.

In this case long term operation could not be obtained due to inadequate mechanical support for the rod. Nevertheless 0.8 watts output at 25 Hz was observed scaling to 2.3 watts from a 0.25 x 3 inch rod. The highest pulse repetition rate attempted was 50 Hz; laser oscillations were observed at this frequency but could not be obtained for extended times.

5.2.2 ROD 446.1a:2% Er:YLF

Long pulse data as a function of repetition rate and input energy was obtained. The pump conditions were:

Rod:	446.1a, 2% Er:YLF, 5.5 x 52 mm
Pump Cavity:	Aluminized Sphere, dia. = 8 inches Liberty Mirror Coating #749
Flashlamp:	ILC 3 x 50 mm, 3000 Torr Xe
Trigger Mode:	Parallel
Energy Storage:	25 μ f, 22 μ H; Pulsewidth 60 μ s FWHM Critically damped
Cooling:	Separate (water) coolant loops over lamp and rod
Resonator:	Plane parallel - external mirrors, no coatings on rod.

The optical quality of this rod (grown in a helium atmosphere) was rather poor; many scattering inclusions were visible throughout the entire length of the rod. Although the parameters described for this experiment are nominally similar to those discussed above, the pumping efficiency in this experiment was considerably better. In particular a new flashlamp was used and the flashlamp/rod separation was smaller.

Figure 19 shows the single shot slope efficiency as a function of mirror reflectivity. Figure 20 shows the output power versus input energy with pulse repetition rate as a parameter. In figure 21 the output power versus repetition rate with input energy as a parameter (output reflectivity = 0.85) is shown. The indicated experimented error is due to the reading error in the power meter; full scale sensitivity = 1.0 watt. A maximum of 0.25 watts output was obtained; at higher input powers a steady output could not be maintained.

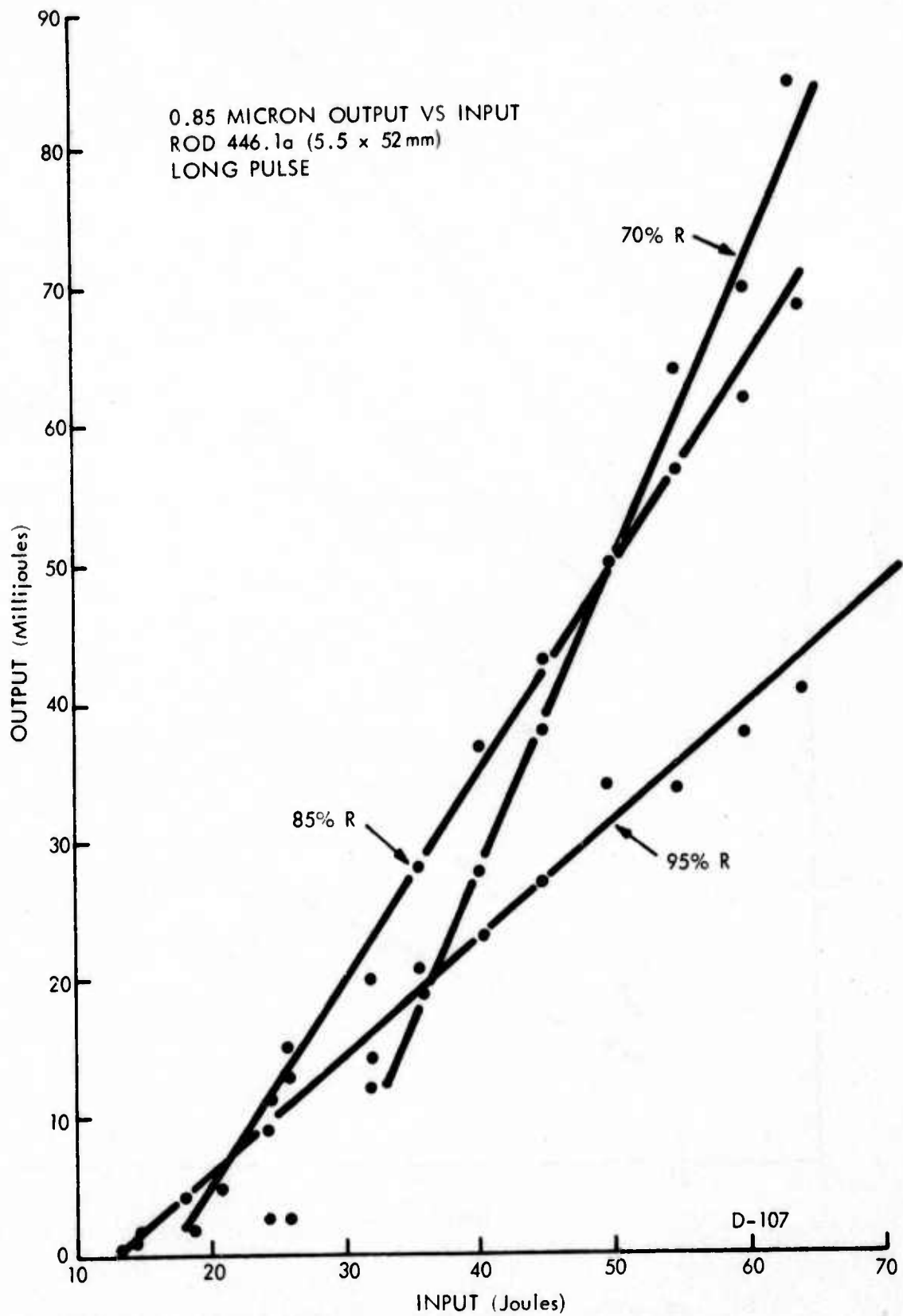


Figure 19 Single Shot Output Vs Input, Rod 446.1a.

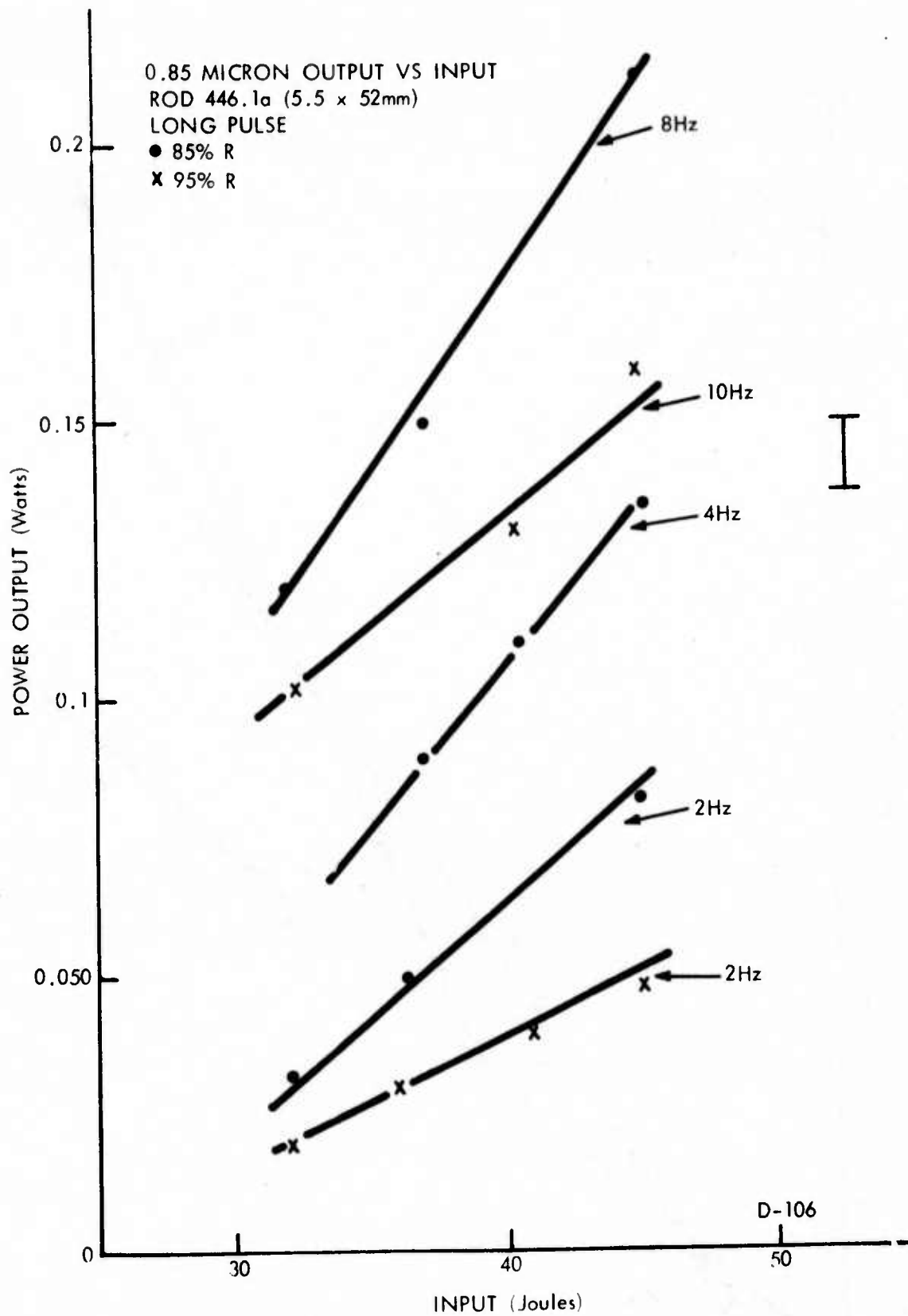


Figure 20 Long Pulse Output Power Vs Input Energy, Rod 446.1a.

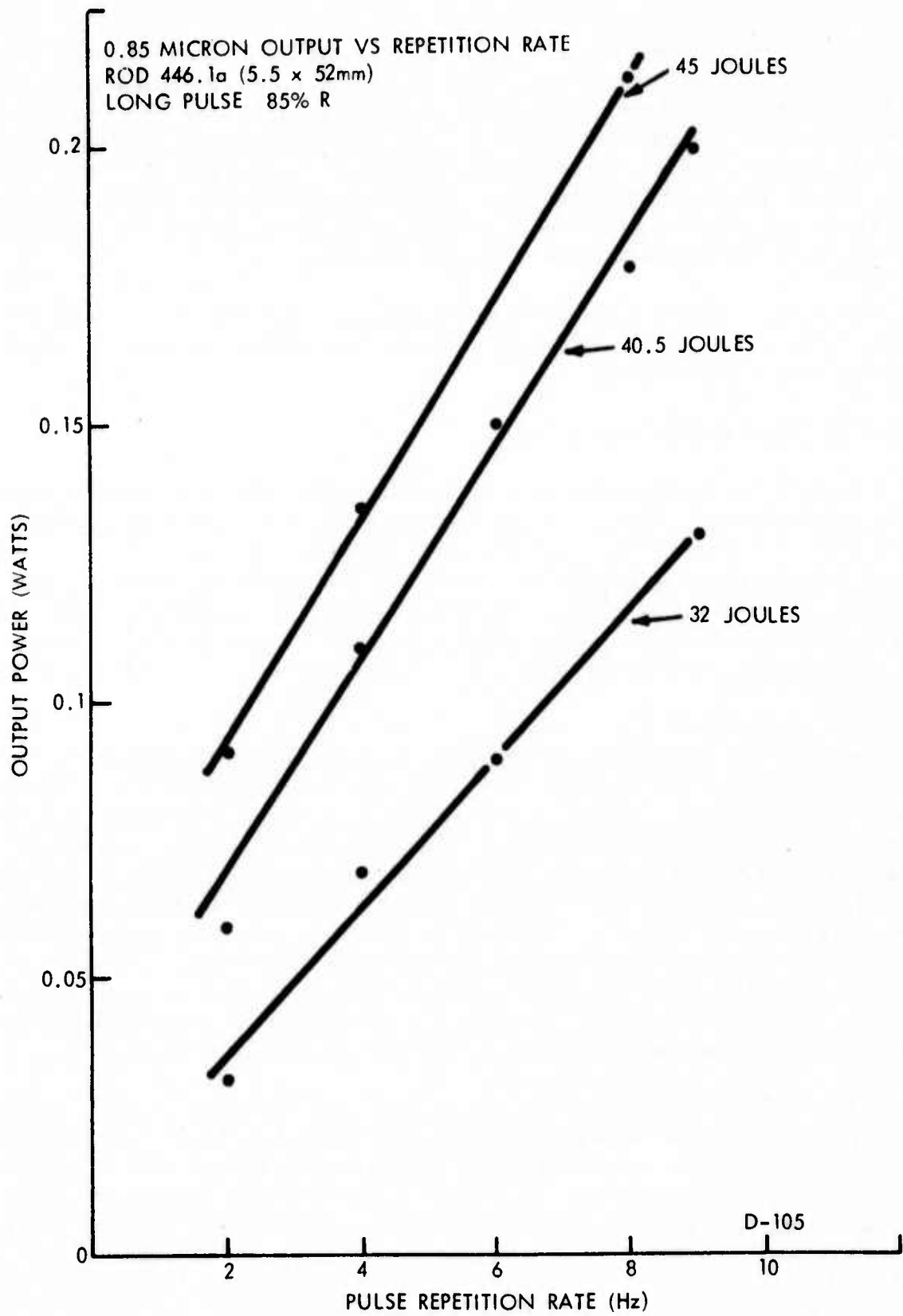


Figure 21 Long Pulse Output Power Vs Repetition Rate, Rod 446.1a.

5.2.3 REMARKS

Comparison of the data of figures 16, 17, and 19 indicates an apparent contradiction, viz: the efficiency of 446.1a:2% Er appears considerably better than 463.4:2.5% Er in water cooled operation (figures 17 and 19) and considerably poorer in an uncooled cavity (figure 16). As mentioned above, however, pump cavity efficiencies utilized in obtaining the data shown in figures 17 and 19 were not the same. However, considerable care was exercised to assure that the data in figure 16 represented performance differences apart from pump cavity effects - i. e., due to Er^{3+} concentration and optical quality.

Evaluation of rods from the last two boules, 3.5% Er and 2.5% Er - .05% Pr is incomplete. From figure 16 substantial improvements in output and efficiency can be anticipated.

5.3 Q-SWITCHING EXPERIMENTS

Q-switching experiments were attempted using calcite polarizers and KD*P electro-optic crystals. In a previous report (4) Q-switched results using a rotating mirror were described. On a parallel company funded program (25) more than one half of the long pulse energy was Q-switched (at the same input energy) using a saturably absorbing Kodak dye embedded in a plastic substrate. In these experiments the maximum output energy observed was 30 mj but multiple spikes were observed. Operation at 10 Hz with a Q-switched average power of 50 mw was obtained.

Electro-optic switching experiments, however, met with very limited success. The source of the difficulties is associated with high losses observed in the calcite polarizer. Comparisons of long pulse outputs with and without the polarizer in the resonator were made. With the polarizer in the resonator (calcite AR coated with MgF_2) the long pulse output was reduced by a factor of 20. Insertion of the KD*P alone (MgF_2 coated windows with index matching fluid for the crystal), resulted in a 10% decrease in the long pulse output. A replacement calcite polarizer was obtained from the vendor but similar results were observed. Q-switched outputs were obtained but the maximum energy output was only 10 mj (60% of the long pulse energy output at the same input with the calcite/KD*P in the resonator) and the overall efficiency very low (0.01%).

Laser emission in Er^{3+} :YLF is π polarized (4) and over a limited range of inputs energy a polarizer is not required. Q-switched outputs of only a few mj in a single spike were obtained using KD*P without a polarizer. The amplitude of giant spikes was approximately an order of magnitude greater than the spikes observed during long pulse oscillations. At $\sim 2 \times$ Q-switched threshold long pulse

oscillation could not be held off, and at higher inputs most of the output energy consisted of long pulse oscillation. This is not surprising, for even in the case of a laser with gain in only one polarization, ($\pi:\sigma:3:1$ in Er:YLF), some polarization selective element must be included in the resonator. Otherwise, for quarter wave retardation on the electro-optic element, feedback is provided after four passes. That is, after the first double pass through the electro-optic material the polarization is rotated by 90° providing no feedback to the assumed linearly polarized laser rod. However, after another double pass the polarization is again rotated - this time parallel to the gain direction of the rod. The effect is simply to double the round-trip resonator loss. Q-switched outputs without long pulse oscillations can then only be obtained near threshold as was observed.

The poor efficiency obtained with calcite in the resonator is attributed to losses in the calcite. The first crystal was found to have "poor transmission at $0.85\mu\text{m}$ " by the vendor, and the second has yet to be analyzed. Calcite appears to be a suitable material at this wavelength (despite our poor results) but alternate polarizing techniques are being investigated. A Brewster plate has been designed but was not available in time for evaluation for this report.

5.4 TERMINAL LEVEL LIFETIME

To date no evidence of the effects of the long terminal lifetime have been observed. It has been shown ⁽⁶⁾ that the only observable effect might occur at high repetition rates where the interpulse period approaches the inverse fluorescence lifetime. Rods of $2.5\% \text{Er}^{3+} - 0.05 \text{Pr}^{3+}$ have been grown for comparative measurements with rods of $2.5\% \text{Er}$. The very dilute Pr^{3+} concentration was chosen to minimize Pr sensitization of $^4\text{S}_3/2$. In this composition it is anticipated that the lower manifold Er^{3+} lifetime will be quenched by at least a factor of 4 and the upper level lifetime will be unaffected. Rods were not received in time for evaluation.

(THIS PAGE INTENTIONALLY LEFT BLANK)

6.0 PERFORMANCE POTENTIAL OF Er:YLF

Based on spectroscopic data, a discussion of anticipated laser performance of Er^{3+} :YLF is presented by contrasting the relevant spectroscopic parameters to those of Nd:YAG.

6.1 PUMPING EFFICIENCY

Figure 22 shows level diagrams of Er^{3+} and Nd^{3+} indicating the similarity of the $^4\text{F}_3/2 \rightarrow ^4\text{I}_{11}/2$ transition in Nd to the $^4\text{S}_3/2 \rightarrow ^4\text{I}_{13}/2$ transition in Er. Both ions have a series of closely spaced absorption bands which feed the upper laser level. In Nd:YAG the feeding rate would be expected to be much faster than in Er:YLF due to the narrower gaps and the higher rate of non-radiative decay in oxide hosts, (26) in general. However, in Er:YLF feeding from levels at least up to $0.36 \mu\text{m}$ ($^4\text{G}_{11}/2$) occurs within $25 \mu\text{s}$, sufficiently fast to be useful.

The major differences in pumping the two materials is the position of the important pump bands:

Nd:YAG	$\sim 0.5 - 0.9 \mu\text{m}$
Er:YLF	$\sim 0.36 - 0.55 \mu\text{m}$

and their relative strengths. On the basis of absorption spectra (see figure 23) the pump bands of Nd:YAG appear to be considerably stronger; this may be overcome through the use of higher Er^{3+} concentrations. A crude estimate of the comparative pumping efficiency of the two materials was obtained by integration of the pump bands (figure 23). Neglecting source variations, we obtain for the normalized integrated absorption in the regions of interest:

1% Nd:YAG:	$1(\lambda \approx 0.45 - 0.9 \mu\text{m})$
2% Er:YLF:	$\sim 0.5(\lambda \approx 0.35 - 0.55 \mu\text{m})$

in relative units for samples of the same thickness. 2% Er:YLF was chosen as it has nearly the same lifetime as Nd:YAG. Source variations were neglected as the emission spectra of, say, Xe flashlamps can be tailored to some extent for

ENERGY LEVEL DIAGRAMS OF Er:YLF AND Nd:YAG

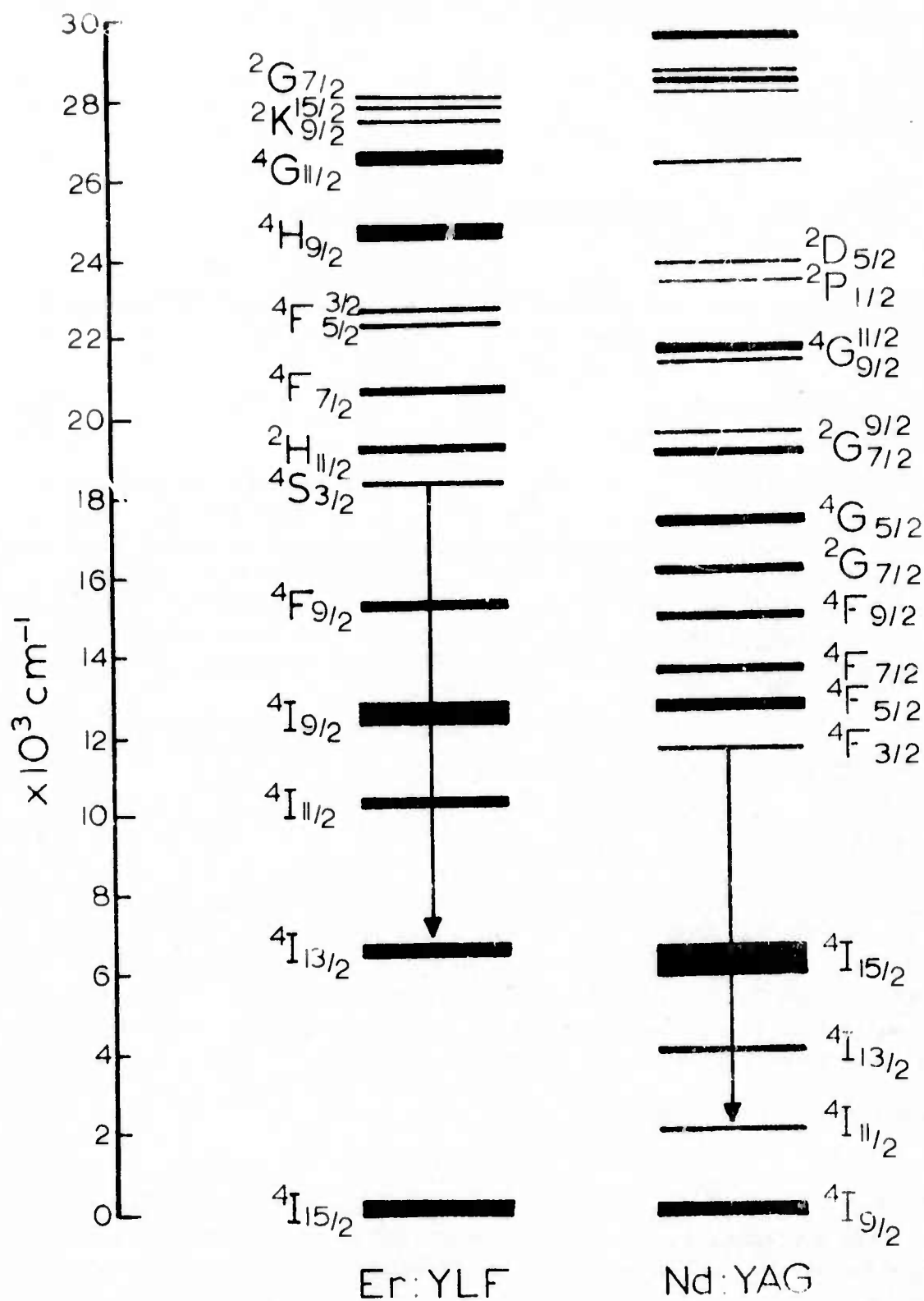


Figure 22 Energy Level Diagrams of Er:YLF and Nd:YAG.

ABSORPTION SPECTRA OF Nd:YAG AND Er:YLF

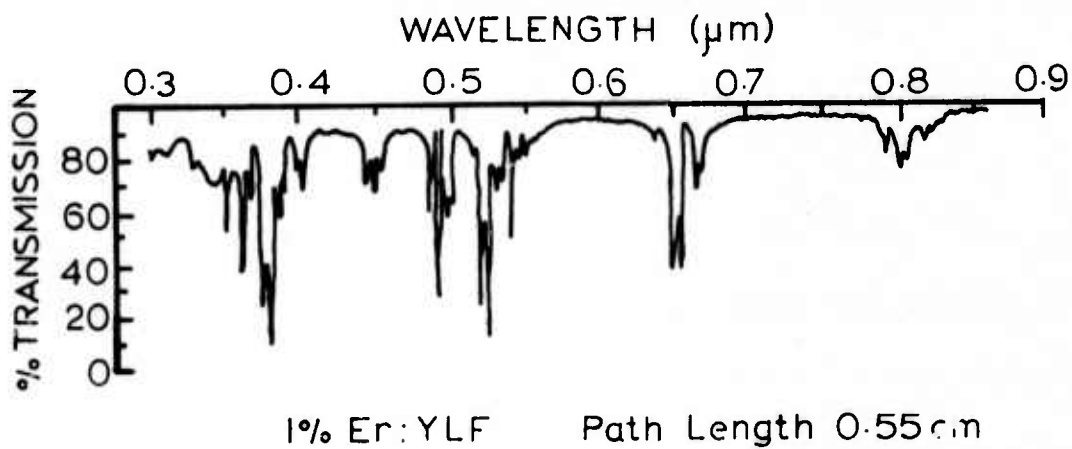
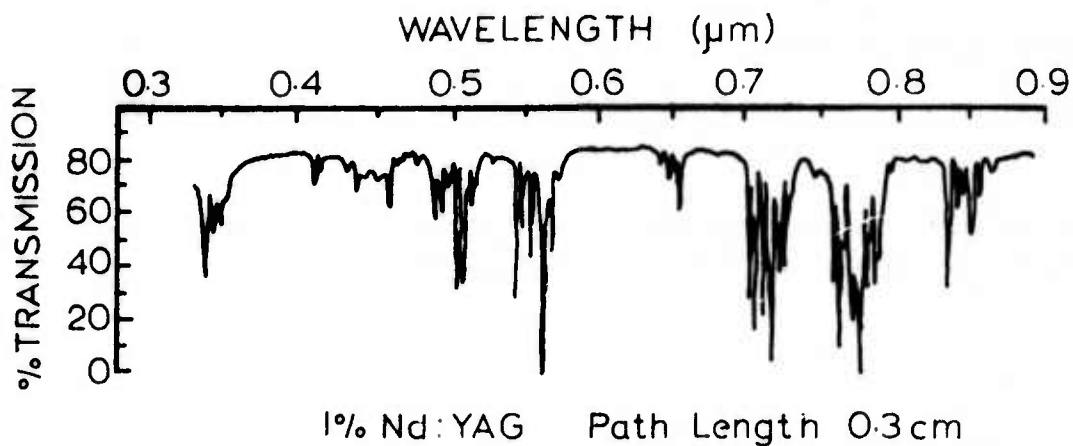


Figure 23 Absorption Spectra of Nd:YAG and Er:YLF.

specific pump regions. (27) Thus the difference in absorption efficiency per unit volume for two materials for these assumptions is roughly 2:1 Nd:YAG:Er:YLF.

6.2 FLUORESCENCE LIFETIMES AND EMISSION CROSS SECTIONS

The fluorescence lifetimes of the upper laser levels of both materials (1% Nd:YAG, 2% Er:YLF) are approximately the same ($\geq 200 \mu\text{s}$) at room temperature. Of course, the radiative lifetime of the laser transitions, as well as the branching ratios, are quite different; these differences affect the transition cross-section (discussed below). However, all other excited levels in Nd:YAG are strongly quenched. As a result, during the pump cycle ions are either in the upper laser level or in the ground state.

In Er:YLF, on the other hand, there are at least three manifolds which are long lived at room temperature. They are:

$${}^4I_{13/2}: 13 \text{ ms}$$

$${}^4I_{11/2}: 4 \text{ ms}$$

$${}^4F_{9/2}: \sim 50 \mu\text{s}$$

Ions pumped to these levels cannot contribute to laser operation and in fact can decrease the absorption strength of the useful pump bands. Thus pumping these levels ($1.8 \mu\text{m} < \lambda < 0.6 \mu\text{m}$) should be avoided.

The stimulated emission cross-sections for the respective laser transitions are:

$$\text{Nd:YAG} - 4.6 \times 10^{-19} \text{ cm}^2 \quad (21)$$

$$\text{Er:YLF} - 1.5 \times 10^{-19} \text{ cm}^2 \quad (\pi \text{ polarization}) \quad (6)$$

6.3 THRESHOLD PARAMETERS

Now the threshold equation for a four level laser is:

$$R \exp 2l(a - \delta) = 1$$

where:

$$a = (N_u - N_l) \sigma, \quad N_l = 0$$

or:

$$N_u = \frac{\ln R}{2l\sigma} + \frac{\delta}{\sigma} \quad (6-1)$$

where:

R = output mirror reflectivity

l = rod length

N_u = upper level population/cm³ at threshold

N_l = lower level population/cm³ at threshold

σ = stimulated emission cross-section

δ = scattering loss (cm⁻¹)

This can be written in the case of R ~ 1 as:

$$N_u \approx \frac{\delta}{\sigma} \quad (6-2)$$

The threshold energy is proportional to the upper manifold population which is related to N_u through the occupation factor of the upper level. The $^4F_{3/2}$ and $^4S_{3/2}$ consist of two levels of approximately equal splitting so we can assume:

$$E_T = K_1 K_2 \frac{\delta}{\sigma}$$

applies for both Er:YLF and Nd:YAG, where E_T is the threshold energy, K_1 accounts for the ratio input energy to flashlamp/photons incident upon laser rod, and K_2 the ratio photons incident on the laser rod/ions excited to the upper laser level. With assumed unit quantum efficiencies for all the pump bands and a spectrally flat source, K_2 is simply proportional to the integrated absorption of the respective materials calculated above.

The ratio of thresholds for 2% Er:YLF and 1% Nd:YAG is then:

$$\begin{aligned} \frac{E_T^*(\text{Er:YLF})}{E_T^*(\text{Nd:YAG})} &\approx \frac{K_2^*}{K_2^*} \frac{\delta^* \sigma^*}{\delta \sigma^*} \approx 2 \frac{\delta^* \sigma^*}{\delta \sigma^*} \\ &\approx 6 \frac{\delta^*}{\delta} \end{aligned} \quad (6-3)$$

Note that K_1 is the same for both materials pumped under the same conditions and the asterisk refers to values of Er^{3+} . Thus the threshold for Er:YLF is expected to be 6 times that of Nd:YAG provided:

- (a) The scattering losses are the same.
- (b) The pump band quantum efficiencies are the same.
- (c) The pump can supply the same photon density in the pump bands of both materials with equal efficiency.
- (d) The effect of the long lived states ($^4I_{13/2}$, $^4F_{9/2}$) in Er:YLF is negligible at threshold; i. e., no depletion of the ground state population.

From Sections 4.0 and 5.0 of this report we note that higher efficiencies are predicted and, indeed, obtained with higher Er^{3+} concentrations. Thus the pump efficiencies of the two materials can be made approximately equal by using 4% Er:YLF. In this case, the upper level lifetime of the Er would be 100 μs requiring relatively short flash pulses to avoid losses of the upper level population due to non-radiative decay. The ratios of thresholds would then be 3:1 : Er:YLF : Nd:YAG.

In Q switched operation, YLF benefits from the fact that the 0.85 μm laser emission is π polarized⁽⁶⁾ and losses to the polarizing element in the resonator should be considerably less than in the case of Nd:YAG. Furthermore, as the stimulated emission cross-section for Er^{3+} :YLF is 1/3 that of Nd:YAG the energy storage limitation due to amplified spontaneous emission⁽²⁸⁾ is approximately a factor of 3 higher. That is for $1/4 \times 3$ inch rods the fundamental limitation of the Q-switched output energy for Nd:YAG is ~0.25 joules, for Er^{3+} :YLF ~0.75 joules.

6.4 EFFECTS OF SCATTERING ON LASER OUTPUT

From the preceding discussion, it is seen that nearly equal pumping efficiencies can be obtained in Er:YLF and Nd:YAG provided equal pump irradiance can be obtained in the spectral regions of absorption of both materials. The difference in cross-sections for both materials can be somewhat compensated for by with mirror reflectivity. We now consider the effect of the remaining parameter, the scattering loss, on laser output following an analysis due to Henningsen.⁽²⁴⁾

Consider a resonator with output coupling R and loss coefficient δ (cm^{-1}). Neglecting diffraction, the loss in a double pass through the resonator due to scattering is given by:

$$1 - \exp(-2\delta l)$$

and the "loss" through the output mirror is:

$$1 - R$$

The fraction coupled out is then simply:

$$f = \frac{1 - R}{1 - R + 1 - \exp(-2\delta l)} \quad (6-4)$$

This is plotted in figure 24 with δ as a parameter. Note that the loss due to scattering is particularly severe when low output coupling (high reflectivity) mirrors are used.

6.5 AN EXTRAPOLATION

Let us consider what the effects of reducing the scattering loss by a factor of four will have on laser output. We consider a 5 cm rod with an assumed scattering loss, δ , of 0.02 cm^{-1} operated with an 85% R output mirror. From equation 6-1 the upper level population (proportional to the threshold) is:

$$N_u = 4.3 \times 10^{17} \text{ cm}^{-3}$$

Under the same conditions with $\delta = 0.005^* \text{ cm}^{-1}$ we have:

$$N_u = 1.4 \times 10^{17} \text{ cm}^{-3}$$

or a reduction in threshold by a factor of 3.

From figure 24 we see that the output at fixed input above threshold will increase by a factor of 1.7, due to the decreased fraction of power coupled out of the resonator.

Figure 19 shows the single shot, long pulse input/output behavior of rod 446.1a taken in a water cooled cavity. Assuming a 2%/cm loss is reasonable for this material, we estimate the performance level for a rod in which the scattering loss is reduced by a factor of four. Using the 85% R data applying the corrections calculated above, we obtain a threshold of ~6 joules with 110 mJ output at 20 joules input using 6-1 and 6-4. Furthermore, as the observed output power was found to be approximately the single shot energy times repetition rate at 10 Hz, we obtain 1.1 watts of output for 200 watts input long pulse at 10 Hz. This corresponds to an overall efficiency of 0.55%. Note that the only assumptions

*The scattering loss of high quality Nd:YAG⁽²¹⁾

EFFECTS OF SCATTERING LOSS ON LASER OUTPUT

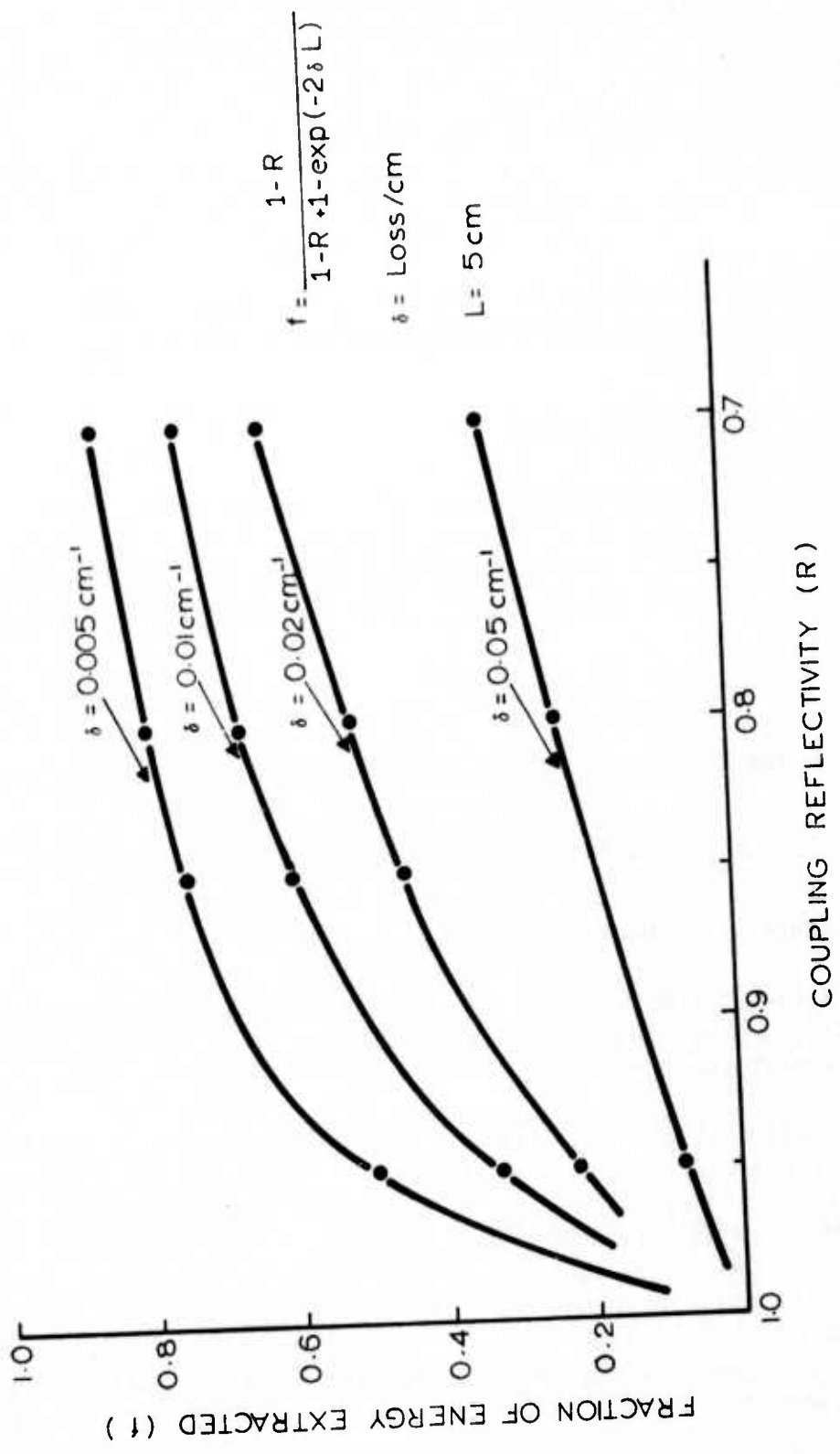


Figure 24 Effects of Scattering on Laser Output.

D-143

involved are rods grown in a He atmosphere exhibit a 2%/cm scattering loss and that this can be reduced by a factor of four. Other potential improvements in performance, particularly improvements in pump cavity efficiency, have not been taken into account.

If we consider the results of Section 5.1 we note that the relative improvement in laser performance obtained with rods of higher Er^{3+} concentration is rather dramatic. For example at 20 joules input the output of the 3.5% rod (470.3) is four times that of the 2% Er rod (446.1a). This reflects the combined effects of the better pumping efficiency and superior optical quality of the rod of higher Er^{3+} concentration. Thus overall efficiencies substantially better than 0.5% are anticipated.

(THIS PAGE INTENTIONALLY LEFT BLANK)

7.0 CONCLUSIONS AND RECOMMENDATIONS

We believe that the major conclusion to be drawn from this investigation is that Er^{3+} :YLF provides a viable alternative to Nd:YAG for certain applications. Use of a 0.85 μm laser is attractive when wavelength diversity or the improved detectivity of photocathode and certain television surfaces at 0.85 compared to 1.06 μm present overall systems advantages. Furthermore, we believe that the development of this material will extend the capabilities of some existing systems (GaAs illuminators, for example) and present the possibility of entirely new systems applications (moderate range covert photography, for example).

This program has demonstrated that large boules of YLF of reproducibly good optical quality can be grown. A dramatic improvement in optical quality and yield of YLF boules has been achieved, the source of previously observed bubble inclusions having been identified and eliminated. A prescription for the elimination of microscopic inclusions, not visible to the unaided eye, has yet to be determined. To this end preliminary experiments conducted with recrystallized feed material have been encouraging. Optical quality comparable to that of YAG has been observed in a recent growth run. Further experiments are required to define the complex inter-relationship between feed purity and growth parameters and their effects on crystalline quality.

Spectroscopic studies have shown that the effect of the long-lived terminal manifold of the laser transition is negligible in single shot operation. For laser operation at high repetition rates the terminal manifold can be strongly quenched (if necessary) by the addition of small amounts of Pr^{3+} without affecting the upper level lifetime. The wavelength of the laser emission ($\lambda = 0.8502 \pm 0.0002 \mu\text{m}$) and the stimulated emission cross section ($\sigma = 1.5 \times 10^{-19} \text{ cm}^2$) have been measured. Studies of the concentration and temperature dependence of the upper laser level lifetime have led to a predicted optimum concentration of 5% for room temperature pulsed operation. Substantially improved efficiencies are predicted at lower temperatures where considerably higher Er^{3+} concentrations can be utilized without severe losses due to "concentration quenching". To complete spectroscopic studies directed at laser material optimization the temperature and concentration dependence of the relaxation rates between the pump bands and the upper laser level should be investigated. In addition some efficiency improvements may result from sensitization. However, the sensitizing species must

exhibit no absorption at $0.85\mu\text{m}$, must feed the upper laser on a time scale short compared to the upper level decay time, and should not quench the upper laser level.

Measurement of most of the physical properties of YLF has been completed. The "thermal figure of merit" for solid state lasers, the thermal load at fracture, is 11 watts/cm and the predicted output power at this input loading in flashpumped operation is 7.6 watts/cm. YLF is relatively soft and the strength of this material is considerably lower than that of typical oxide hosts. Nevertheless, the material presents no unusual fabrication problems; internal laser damage has not been observed; and the material is, for all practical purposes, immune to flashlamp induced damage. For complete definition of the physical properties of YLF thermal lensing (dn/dt) and the stress-optic coefficients should be determined.

Laser testing was primarily directed at demonstrating the feasibility of the material for moderate average power applications. Room temperature (water cooled) operation at up to 50 Hz was demonstrated with a maximum output power of 0.8 watts at 25 Hz. Scaling power proportional to volume we obtain 2.3 watts for a 0.25×3 inch rod. Laser measurements showed improved efficiencies with Er^{3+} concentration over the range 2 - 3.5%. Reasonable extrapolations from laboratory dates indicate operating efficiencies greater than 0.5% at 10 Hz are available with existing material. Insufficient Q-switch data was obtained (due to problems discussed in the text) for definition of performance parameters. However as laser oscillations are strongly π polarized the difference between Q-switched and long pulse efficiencies are expected to be less than in Nd:YAG. The optimum pump conditions have not been systematically investigated. In particular as the pump bands lie in the region $\lambda < 0.55 \mu\text{m}$, sources with good emission and pump cavity walls with good reflectivity in this region are desirable. One approach which appears particularly promising is the use of dye laser flashlamps which exhibit high blue-ultraviolet irradiance and permit the use of high Er^{3+} dopant levels without degradation to "concentration quenching".

APPENDIX

PHASE DIAGRAMS AND CRYSTAL GROWTH

The phase diagram is a graphical representation of the equilibrium relationships between system composition and temperature which shows what phases will be in equilibrium under any conditions, and also implies the number of degrees of freedom for these conditions. In systems little affected by pressure, this variable is neglected.

One of the prime uses of phase diagrams is in illustrating behavior during crystallization from a melt. Conversely, careful observation of an experimental crystallization can illuminate details of a phase diagram not fully clarified by other methods (DTA and X-ray). Two types of crystallization paths can be considered. The first, called equilibrium freezing, requires a closed system, no thermal gradients, and complete equilibrium between liquid and solid at any temperature. Normal freezing is the path usually encountered during crystal growth. It allows an open system, and thermal as well as concentration gradients.

It is interesting to look in some detail at the system LiF-YF₃. This diagram, determined by Thoma et al., Figure 25 is a simple type i. e., two components and one incongruently melting intermediate compound. The system characteristics are as follows: 1) A eutectic between liquid, LiF and LiYF₄ at 19 mol % YF₃, 2) a peritectic between YF₃-LiYF₄ and liquid at 49 mol %, YF₃ at 819°C and 3) a phase transition in solid YF₃ at 1052°C. Two general features are the liquidus and solidus lines. The former is the temperature at which solid phase will first appear when liquid of any composition in the single phase region is cooled. As the system temperature is further lowered, the proportion of solid to liquid phase will increase until the liquid phase disappears. This temperature at which the last fraction of liquid disappears is called the solidus. If one draws a horizontal tie line (constant temperature) on a binary phase diagram connecting a liquidus with its corresponding solidus this will indicate the compositions of the phases in equilibrium. For example, at 750°C a liquid of composition 70% LiF will be in equilibrium with solid LiYF₄.

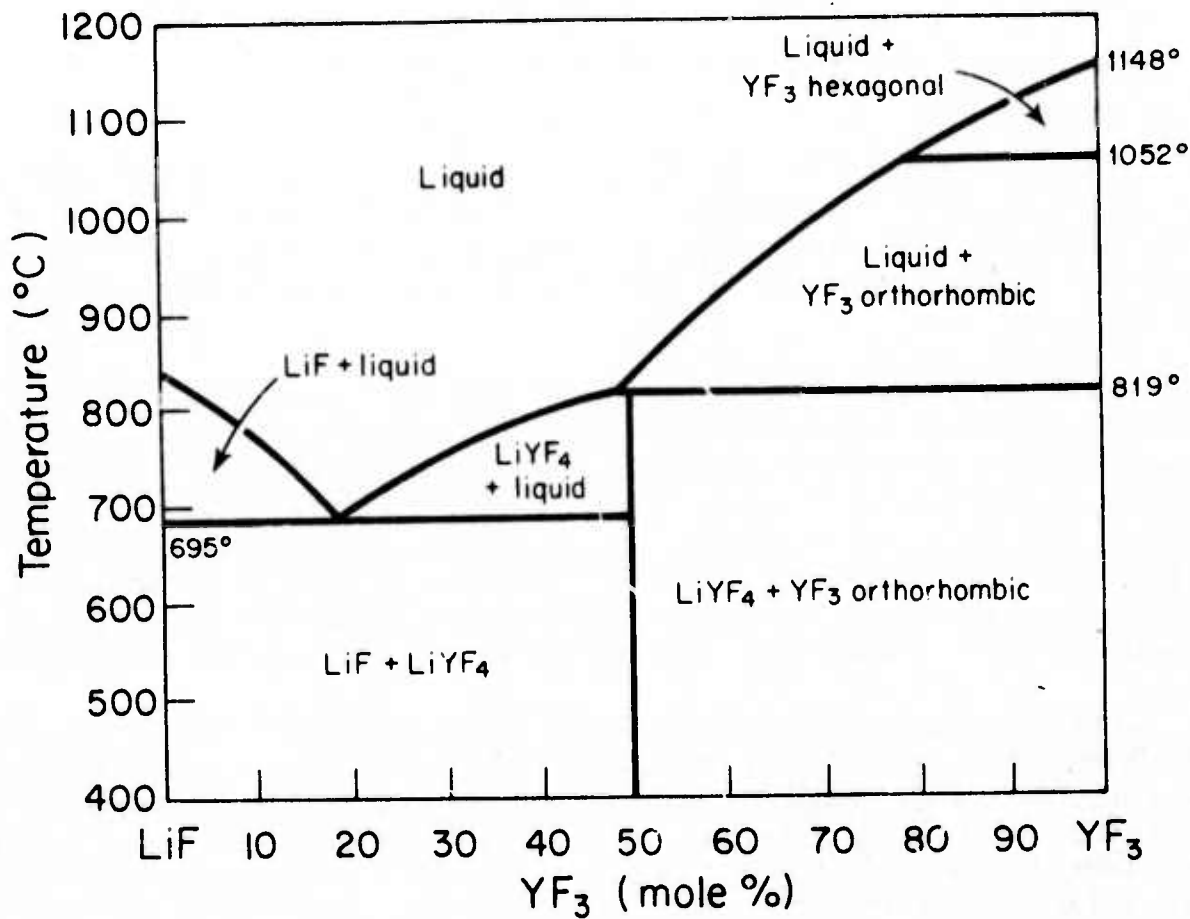


Figure 25 Phase Diagram of LiF-YF₃ System.

Lithium yttrium fluoride is incongruently melting. That is, if a specimen of solid LiYF_4 is heated, its temperature will increase until the peritectic temperature, 819°C , is reached. At this point, solid LiYF_4 will decompose to a liquid of composition 49% YF_3 and to solid YF_3 . Exactly enough heat is absorbed during this transition to prevent a temperature rise. According to the phase rule, for a two-component reduced system, three phases in equilibrium represent an unvariant point. That is, as long as three phases remain in equilibrium, the temperature cannot be changed by addition or subtraction of heat. With further addition of heat, LiYF_4 will continue to react to form liquid of composition 49% YF_3 and solid YF_3 . When the last trace of LiYF_4 has reacted, the system temperature may again rise. Yttrium fluoride will now dissolve in the liquid, enriching it (YF_3 will be in equilibrium with the liquid) until it has attained the composition 50% LiF 50% YF_3 , at which point there will no longer be present solid YF_3 . The system will now be a single phase liquid with the system composition. Upon cooling under equilibrium conditions, the path just described will be followed in reverse order.

Normal freezing conditions give rise to differing behavior. It is important to realize that crystals grown at "equilibrium" are actually grown under steady state conditions approximating normal freezing. If a melt with a composition 50% LiF , 50% YF_3 , is cooled, the first solid phase to form is YF_3 . As heat is withdrawn, more YF_3 forms, the liquid is enriched in LiF , and the system temperature falls. When the liquid reaches the peritectic composition, solid YF_3 will react with the liquid to form LiYF_4 , which then covers the pre-existing solid YF_3 . The system will then be free to crystallize along the liquids extending from the peritectic to the eutectic, with solid LiYF_4 crystallizing while the liquid becomes richer in LiF . When the liquid attains the eutectic composition, LiF and LiYF_4 will crystallize in proportions dictated by that composition. The remainder of the melt, then, will crystallize without change in either temperature or composition. After the last trace of liquid has solidified, the system temperature will again be free to fall.

In a real crystal growth experiment, passage from one solid phase field to the next will be characterized by sharp boundaries parallel to the growth plane. For example, in growing a crystal (nucleated on a wire) from the 50/50 melt through the peritectic, one will observe an initial clean, single-phase portion of YF_3 , followed by a sharply delineated two-phase region consisting of YF_3 and LiYF_4 and characterized by an almost opaque, highly polycrystalline appearance. Following this will be a clean single phase region of LiYF_4 . When the eutectic composition is reached, a sharp boundary will form, separating LiYF_4 from the LiYF_4 - LiF eutectic mixture. The actual amount of eutectic mixture will be small, owing to the fact that crystallization of single phase LiYF_4 begins at the peritectic composition. In a real crystal growth situation, the crystallization of the peritectic mixture will persist over a finite length of boule, as a result of the prevailing

steady state conditions. Again, in growing a real crystal, to avoid crystallization through a peritectic region which would preclude seeded single crystal growth of LiYF_4 , the starting melt composition is chosen on the slightly LiF-rich side of the peritectic. In addition, to avoid the physical problems encountered when growing from a very shallow melt, crystallization of LiYF_4 is never brought down to the eutectic.

If crystal growth or normal freezing were commenced from a melt containing greater than 50% YF_3 , but not 100%, the same crystallization path would be followed and the mass of YF_3 deposited would increase as the fraction of YF_3 in the system increases.

The rare earths from Er to Lu form congruently melting compounds with LiF. A phase diagram typical of this behavior is shown in figure 26. LiErF_4 is congruently melting. Thus a specimen of LiErF_4 when heated to its congruent melting point melts at a fixed temperature to a liquid of the same composition as the solid. Conversely, from a melt of 50% LiF and 50% ErF_3 when cooled to the liquidus, LiErF_4 would crystallize. Since the solidus and liquidus coincide at a congruent melting point, continued withdrawal of heat from the system will result in a crystallization of the total mass of the system as LiErF_4 with neither a change in temperature nor melt composition, even though only two phases are in equilibrium.

Crystallization from melts with a composition either side of the 50/50 line, but within the LiErF_4 phase field, will result in the formation of LiErF_4 as the first solid phase, and concomitant enrichment or depletion of the melt in LiF (or YF_3) according to initial melt composition. Accordingly, as crystallization of LiErF_4 proceeds, the temperature will also fall. When one or the other of the eutectic compositions is reached, crystallization of the respective eutectic composition will begin.

In growing a real crystal from a stoichiometric melt in a congruently melting system, the yield is limited by physical conditions such as the depth of the remaining liquid phase.

Crystal growth runs in various LiF- ReF_3 systems have with minor exceptions agreed with the published phase equilibrium. In the system LiF- YF_3 growth from a stoichiometric melt yielded a succession of phases characteristic of an incongruently melting system. Further crystal growth experiments indicate that the peritectic lies between 50 and 52 mole % LiF. LiYF_4 is normally grown from a melt starting at 52 mole % LiF.

In the system LiF- YF_3 - ErF_3 - HoF_3 - TmF_3 up to about 50% ErF_3 , crystal growth experiments indicate incongruent behavior with the peritectic of about 51%

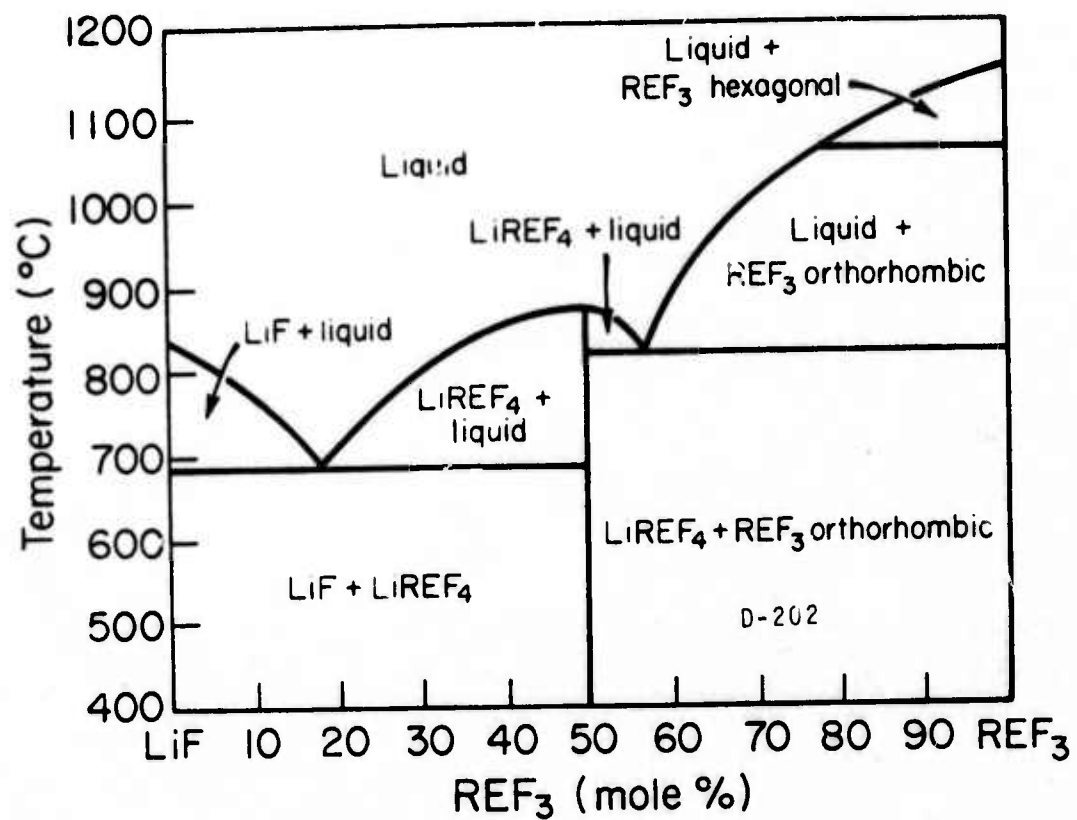


Figure 26 Phase Diagram Typical of Congruently Melting LiF-REF₃ Compounds.

LiF. Pure LiErF_4 has been shown in zone refining experiments to be congruently melting, while zone refining experiments on LiYF_4 have confirmed the incongruent behavior. Congruently melting LiYbF_4 has been pulled from a YbF_3 rich (53%) melt. The succession of phases, LiYbF_4 followed by a mixture of LiYbF_4 and YbF_3 indicates congruent behavior. In the systems LiF-TbF_3 and LiF-GdF_3 our experiments were in minor disagreement with the published phase diagrams in the composition of the peritectic; it was found to be richer in LiF than reported. These observations have been reconfirmed in all the crystal growth experiments conducted in this laboratory.

In summary, the agreement between crystal growth experiments and behavior predicted from published phase diagrams has been excellent.

REFERENCES

- (1) E. P. Chicklis, C.S. Naiman and A. Linz, "Stimulated Emission at 0.85 μm in $\text{Er}^{3+}:\text{YLF}$ ", Dig. Tech. Papers, Seventh Int. Quantum Electronics Conference, 17, May 1972.
- (2) E. P. Chicklis and C.S. Naiman, "A Review of Near Infra-Red Optically Pumped Solid-State Lasers", Proc. First European Electro-Optics Markets and Technology Conference, IPC Science and Technology Press Ltd., Guildford, Surrey, England, 77, 1973.
- (3) V. Belruss, J. Kalnajs, A. Linz, and R.C. Folweiler, Mat. Res. Bull, Vol. 6, 899 (1971).
- (4) E. P. Chicklis, R.C. Folweiler, C.S. Naiman, A. Linz, H.P. Jenssen, D.R. Gabbe, ".85 Micron Solid State Laser Material Evaluation", AFAL-TR-73-94, Contract No. F33615-72-C-2065, April 1973.
- (5) E. P. Chicklis, R.C. Folweiler, C.S. Naiman, A. Linz, H.P. Jenssen, D.R. Gabbe, "Development of Multiply Sensitized $\text{Ho}:\text{YLF}$ as a Laser Material", TR ECOM-00013-F, ARPA Order No. 1868, Contract No. DAAB07-71-C-0013, January 1973.
- (6) E. P. Chicklis, R.C. Folweiler, C.S. Naiman, A. Linz, H.P. Jenssen, D.R. Gabbe, ".85 Micron Solid State Laser Material Evaluation" (Part II), AFAL-TR-73-94, Contract No. F33615-72-C-2065, April 1973.
- (7) H.P. Jenssen, D. Castleberry, D. Gabbe and A. Linz, "Stimulated Emission at 5445A in $\text{Tb}^{3+}:\text{YLF}$ ", Paper 8.4 Presented at the 1973 IEEE/OSA Conference on Laser Engineering and Applications, Washington, D.C., 20 May-1 June 1973.
- (8) A.L. Harmer, A. Linz, and D. Gabbe, J. Phys. Chem. Solids 30, 1483 (1969).
- (9) E.J. Sharp, D.J. Horowitz, and J.E. Miller, J. Appl. Phys. 44, No. 12, 5399 (1973).
- (10) R.L. Remski, L.T. James, K.H. Goen, B. DiBartolo and A. Linz, IEEE J. Quantum Electronics QE-5, No. 4, 214, 1969.
- (11) E. P. Chicklis, J.C. Doherty, R.C. Folweiler, C.S. Naiman, D.R. Gabbe, H.P. Jenssen and A. Linz, "New Results in Optically Pumped YLF IR Lasers". Post deadline paper presented at IEEE/OSA Conference on Laser Engineering and Applications, Washington, D.C., (June 1973).

- (12) R. Pastor, Symposium on Optically Pumped Solid State Lasers, Fort Monmouth, N.J., Oct. 1973.
- (13) R. Uhrin, R.F. Belt, R.C. Puttbach, and D.R. Kinloch, "Preparation and Single Crystal Growth of LiYF_4 Laser Materials", Final Report Contract No. N00014-70-C-0379, Model No. P00003, (Feb. 1974).
- (14) V. Evtuhov, D.P. Devor, B.H. Soffer, M. Robinson, R.C. Pastor, G.E. Moss, and A.G. Hastings, "Solid State Infrared Laser Devices", AFAL-TR-70-221, Nov. 1970.
- (15) T.G. Stoebe, J. Phys. Chem. Solids 28, 1375 (1967).
- (16) E.P. Chicklis, C.S. Naiman, R.C. Folweiler, D.R. Gabbe, H.P. Jenssen and A. Linz, "Development of Multiply Sensitized Ho:YLF as a Laser Material", Final Report, Contract DAAB07-73-C-0066, 1974 (in press).
- (17) G.D. Baldwin, "Q-Switched Evaluation of CaLaSOAP:Nd", Technical Report AFAL-TR-72-334 (September 1972).
- (18) K.B. Steinbruegge, R.H. Hopkins, G.W. Roland et. al. "Increased Energy Storage Neodymium Laser Material: Silicate Oxyapatite", Tech. Report AFAL-TR-72-37, May 1972.
- (19) W.A. Shand, J. Crystal Growth 5, 143 (1969).
- (20) H. Philipp, General Electric Corporate Research Center, Schenectady, N.Y., (private communication).
- (21) R.B. Chesler and S. Singh, J. Applied Phys. 44, No. 12, 544 (1973).
- (22) M.J. Weber, M. Bass, T.E. Vartimos, and D.P. Bua, IEEE J. Quantum Electronics QE-9, No. 11, 1079 (1973).
- (23) H.P. Jenssen, "Phonon Assisted Laser Transitions and Energy Transfer in Rare Earth Laser Crystals", Crystal Physics Laboratory Technical Report No. 16, Center for Material Sciences and Engineering, Mass. Inst. of Technology (September 1971).
- (24) R.H. Hopkins, et al, "Rare Earth Doped Apatite Laser Materials", Technical Report AFAL-TR-71-110 (1971).
- (25) Sanders Associates IR&D Task NWC, "0.85 Micron Laser Illuminator", unpublished results.

- (26) L.A. Riseberg, H.W. Moos and W.D. Pastlow, IEEE J. Quantum Electronics QE-4, No. 10, 609 (1968).
- (27) J.R. Oliver and F.S. Barnes, IEEE J. Quant. Electronics QE-5, No. 5, 232 (1969).
- (28) B. Steinbruegge, T. Henningsen, R.H. Hopkins, et al, Applied Optics 11, No. 5, 999 (1972).

UNCLASSIFIED

Security Classification

DOCUMENT CONTROL DATA - R & D		
<i>(Security classification of title, body of abstract and indexing annotation must be entered when the overall report is classified)</i>		
1. ORIGINATING ACTIVITY (Corporate author) Sanders Associates, Inc. 95 Canal Street Nashua, New Hampshire 03060		2a. REPORT SECURITY CLASSIFICATION Unclassified
		2b. GROUP N/A
3. REPORT TITLE 0.85 Micron Solid State Laser Material Evaluation		
4. DESCRIPTIVE NOTES (Type of report and inclusive dates) Technical Report, 5 December 1972-5 June 1973		
5. AUTHOR(S) (First name, middle initial, last name) Evan P. Chicklis, David R. Gabbe, Robert C. Folweiler, Charles S. Naiman, Hans P. Jenssen, and Arthur Linz		
6. REPORT DATE June 1974	7a. TOTAL NO. OF PAGES 76	7b. NO. OF REFS 28
8a. CONTRACT OR GRANT NO. F33615-72-C-2065	9a. ORIGINATOR'S REPORT NUMBER(S) N/A	
b. PROJECT NO. 2075	9b. OTHER REPORT NO(S) (Any other numbers that may be assigned this report)	
c.		
d.		
10. DISTRIBUTION STATEMENT Distribution limited to United States Government Agencies only; by reason of inclusion of test and evaluation data; applied 3-19-74 ^{Oct 28 1973} Other requests for this document must be referred to AFAL/TEO, Wright-Patterson AFB, Ohio 45433.		
11. SUPPLEMENTARY NOTES	12. SPONSORING MILITARY ACTIVITY Advanced Research Projects Agency Materials Science Directorate 1400 Wilson Blvd., Arlington, Va. 22209	
13. ABSTRACT ABSTRACT		
<p>This third semi-annual report describes the final phase of the program for the development of a 0.85 micron optically pumped laser material: Er³⁺:YLF. Laser operation is obtained at room temperature in this material via stimulated $^4S_{3/2} \rightarrow ^4I_{13/2}$ transitions. Er:YLF is a true four-level laser.</p> <p>The relationship between growth parameters and feed purity and their effects on crystalline quality were investigated. Dramatic improvement in optical quality was obtained in growth runs using argon as the furnace cover gas. Preliminary evidence of further improvements in crystalline quality (comparable to Nd:YAG) resulted from the use of recrystallized feed.</p> <p>The physical properties of YLF are reviewed and the results applied to a calculation of the thermal loading at fracture of a YLF rod uniformly heated and cooled at the surface. The calculated value is 11 watts/cm at thermal fracture corresponding to predicted output power of 7.6 watts/cm.</p> <p>Spectroscopic studies focused on the effects of increased Er³⁺ concentration on laser efficiency. The temperature and concentration dependence of the lifetime of the upper laser level were measured. In flashpumped operation at room temperature an optimum concentration of approximately 5% is predicted.</p> <p>Comparative measurements show significantly improved laser efficiency with Er³⁺ concentration over the range 2-3, 5%. Improved laser performance was observed using rods grown in argon. A maximum output power of 0.8 watts at 25 Hz and a maximum repetition rate of 50 Hz was observed. For a 0.25 x 3 inch rod in excess of 2 watts are obtained by scaling the output with active volume. Overall efficiencies greater than 0.5% at 10 Hz are extrapolated from laboratory data.</p>		

DD FORM 1 NOV 65 1473

UNCLASSIFIED
Security Classification

14

KEY WORDS

LINK A

LINK B

LINK C

ROLE

WT

ROLE

WT

ROLE

WT

0.85 Micron Laser
Laser Material Evaluation
Er:YLF
Erbium
Stimulated Emission
Top Seeded Solution Technique
Four Level Laser
Optically Pumped Laser
Lithium Yttrium Fluoride
YLF
IR Laser
IR Illuminator
Fluoride Laser Material